JOURNAL OF GEOPHYSICAL RESEARCH, VOL. 99, NO. E8, PAGES 17,075–17,094, AUGUST 25, 1994

Auroral Lyman α and H_2 bands from the giant planets: 1. Excitation by proton precipitation in the Jovian atmosphere

Daniel Rego and Renée Prangé[1]
Institut d'Astrophysique Spatiale, Université Paris XI, Orsay, France

Jean-Claude Gérard
Institut d'Astrophysique de Liège, Liège, Belgium

Abstract. This paper is part of a work aimed at modeling the ratio of the observed Jovian auroral intensity at H Lyman α and in the H_2 Lyman and Werner bands and interpreting them as diagnostic of the incident magnetospheric particle species and energy. The work is planned in three steps: (1) modeling of the volume excitation rate, (2) modeling of the radiative transfer at Lyman α, (3) application to existing observational data and new data obtained from the Hubble Space Telescope. The present paper deals with the first step. Models of the volume excitation rate have previously been developed for low energy electrons and oxygen ions. However, the energy range of the study has to be extended towards higher energy in view of recent results on the penetration depth of the primary particles. Protons have not been modeled so far. We have used an existing electron code of degradation of energy [*Gérard and Singh*, 1982] which has been improved, updated and adapted to the case of precipitating protons. The issues of nonequilibrium beam H/H^+ fractions and of getting reliable cross sections over a wide energy range have been considered with particular care. The altitude distribution of the volume excitation rate is compared for electrons and protons, for various initial energies in the range 10-50 keV and 50 keV to 1 MeV, respectively.

1. Introduction

Intense Jovian auroral emissions have been recorded almost simultaneously by the Ultraviolet Spectrometer (UVS) instrument onboard the Voyager spacecraft [*Broadfoot et al.*, 1979] and IUE [*Clarke et al.*, 1980]. They were observed in the far ultraviolet, in the H Lyman α line and H_2 Werner and Lyman bands. The excitation of the atmospheric species (dominated by molecular and atomic hydrogen) was attributed to collisions with energetic charged particles precipitating from the Jovian magnetosphere. In the absence of reliable information on the extent of the auroral region, the estimates of the brightness were rather uncertain, ranging from 60 kR of Lyman α and 80 kR of H_2 bands, assuming a 6000-km-wide auroral oval [*Sandel et al.*, 1979] and 42 kR of Lyman α [*Clarke et al.*, 1980] to a few kR of Lyman α when the emission is assumed to fill the IUE apertures [*Clarke et al.*, 1980]. Very recent novel observations obtained with the Faint Object Camera (FOC) onboard the Hubble Space Telescope (HST) have provided the first insights on the actual geometry of the aurorae. Preliminary results from the north aurora reveal brighter auroral emissions (≈ 180 kR at Lyman α, and ≈ 450 kR in the H_2 bands), confined to more restricted areas (oval width ≈ 100-3500 km) according to *Dols et al.* [1992] and *Gérard et al.* [1993]. All these results, however, lead to a converging estimate of the total energy radiated by the aurorae, in the range of a few times 10^{12} W. The energy input into the atmosphere, derived from the radiated UV flux, ranges from a few times 10^{13} to a few times 10^{14} W, depending on the assumptions [*Yung et al.*, 1982; *Thorne*, 1983; *Livengood et al.*, 1992; *Gérard et al.*, 1993]. This considerable amount of energy gives rise to very important consequences in terms of heating, and changes in the composition and dynamics of the atmosphere. It also proves that the auroral atmosphere is a significant sink for energetic magnetospheric particles, in relation to the global dynamics of the Jovian magnetosphere. Considering the very small body of direct in situ observations (the Pioneer 10 and 11, Voyager 1 and 2, and Ulysses encounters), identification of the nature, energy, and origin of the auroral precipitating particles would be a major step in the understanding of the magnetospheric processes.

In the Jovian magnetosphere, populations of suprathermal and energetic electrons, protons, and heavy ions (especially iogenic sulfur and oxygen) have been detected in significant amounts [*Krimigis et al.*, 1979; *Belcher et al.*, 1981; *Amstrong et al.*, 1981; *Geiss et al.*, 1992; *Lanzerotti et al.*, 1992; *Simpson et al.*, 1992]. The radial distribution of the phase space densities of energetic heavy ions and electrons exhibits the characteristics of inward radial diffusion beyond a limit where a dramatic decrease is observed. The steep gradient, at about 5.2-5.5 R_J for electrons [*Lanzerotti et al.*, 1981] and between 6 and 12 R_J for ions, depending on the authors [*Thomsen et al.*, 1977; *Krimigis et al.*, 1979; *Cheng et al.*, 1983; *Gehrels and Stone*, 1983; *Thorne*, 1983; *Paonessa*, 1985; *Summers et al.*, 1989] has been interpreted as evidence of particle losses by wave-particle scattering and

[1]Also at Institut d'Astrophysique de Paris, Paris, France.

Paper number 93JE03432.
0148-0227/94/93JE-03432$05.00

precipitation into the atmosphere, an interpretation which was consistent with the observed approximate latitude of the aurorae.

In the early studies, only electron precipitation was considered (probably under the influence of the terrestrial example) [e.g., *Waite et al.*, 1983]. But it rapidly appeared that the energy available in the electron population was insufficient, and resonant pitch-angle scattering of protons was first proposed as an alternative [*Goertz*, 1980]. *Thorne* [1981] suggested that heavy ions could be the major component of the precipitated population, and from the analysis of the electromagnetic waves recorded by Voyager, *Thorne* [1983] and *Thorne and Scarf* [1984] gave evidence that resonant scattering of ions by ion-cyclotron waves was much more efficient than scattering of electrons (either by the observed electrostatic or electromagnetic waves) in providing large precipitating energy fluxes. However, even the estimate of the energy input available from the precipitation of ions fell short in accounting for the auroral energy input, suggesting that combined (even though independent) precipitation of all kinds of energetic charged particles could possibly occur.

If the Jovian aurorae are diffuse, this conclusion is supported by the comparison of the longitudinal variation of the observed auroral emission with the variation of the precipitating flux of magnetospheric particles in the asymmetric Jovian magnetic field [*Prangé and Elkhamsi*, 1991; *Prangé*, 1991]. In addition to being both electrons and ions (or protons), the particles should be injected on different L shells ($5 \leq L < 7$ for the electrons, $7 \leq L$ for the ions) to fit the observations.

The observation of X ray emissions by the Einstein satellite was first considered as evidence for heavy ions precipitation [*Metzger et al.*, 1983], but it now seems that electrons can also be efficient in producing X rays [*Barbosa*, 1990]. Nevertheless, the signature of recombination lines of sulfur and oxygen ions has again been identified in soft X ray spectra from the Röntgen satellite (ROSAT) [*Waite and Boice*, 1992]. Even the most recent in situ observations from the Ulysses flyby of Jupiter do not provide a simple answer. The background contribution to the hard X ray signal was too large to allow for the detection of a Jovian contribution, and the 3 σ limit does not rule out electron precipitation.

In addition, an in situ signature of wave particle interactions has been recorded by the plasma wave instrument onboard Ulysses in the inner magnetosphere near L = 7 [*Lin et al.*, 1993] and L = 12 [*Blake et al.*, 1992], whereas strong field-aligned currents and parallel electron beams have been observed on high-latitude field lines [*Balogh et al.*, 1992; *Lanzerotti et al.*, 1992]. The latter could be related to the strong high-latitude Jovian decametric (DAM), hectometric (HOM) and broad kilometric (bKOM) radio source, and to impulsive electrostatic emission at radial distances between 10 and 30 R_J identified by *Barbosa et al.* [1981] and attributed to an inverted-V-type precipitation process (involving electrons and ions).

As for the energy, again a wide range of possibilities is proposed, involving electrons as well as protons or ions in various energy bands from a few keV to several MeV, insofar as wave interaction is concerned [*Thorne*, 1983; *Gehrels and Stone*, 1983]. The existence of precipitating electrons in the 1-10 keV range is anticipated from the observation of auroral radio emission if it is generated through the cyclotron maser instability as generally assumed [*Wu et al.*, 1982; *Le Quéau et al.*, 1984; *Louarn et al.*, 1990], whereas the ion lines in the X ray range suggest that the precipitating ion energy could exceed 700 keV/nucl. [*Waite and Boice*, 1992].

Finally, another approach used by several authors consists of trying to characterize the particles impinging on the Jovian atmosphere through the aeronomic consequences of the precipitations: the ionization, dissociation, and heating of the atmospheric species have been computed for electron and ion precipitations, as well as the excitation of the optical emissions [*Gérard and Singh*, 1982; *Waite et al.*, 1983; *Horanyi et al.*, 1988; *Waite et al.*, 1988]. Their predictions can, in principle, be compared to observations of the atmospheric and ionospheric composition and temperature, and of the auroral emissions. However, remote sensing data of the atmosphere and ionosphere are very rare and partial. In particular, occultation data are hardly available for the auroral regions. The excitation of the species in the upper atmosphere can give rise to emission in the FUV, at Lyman α, and in the H_2 Lyman and Werner bands for the hydrogen. The presence of the UV lines of neutral and ionized oxygen and sulfur can also be anticipated if such heavy ions are precipitating. In addition to the Voyager observations, remote sensing of these emissions has been regularly made by the IUE since their discovery 12 years ago, and the Hubble Space Telescope, which just performed its first UV auroral observations [*Dols et al.*,1992; *Gérard et al.*, 1993; *Trafton*, 1992], will pursue this survey. The altitude distribution of the volume excitation rate at Lyman α, and in the H_2 Lyman and Werner bands were derived by *Gérard and Singh* [1982] in the energy range 0.1-10 keV in the case of electron aurorae. The altitude distribution of the volume excitation rate in the H_2 Lyman bands and column integrated efficiency of the various energy deposition processes (in particular at Lyman α, and in the H_2 Lyman and Werner bands) were derived by *Waite et al.* [1983] for electrons of 1 keV and 10 keV, and by *Horanyi et al.* [1988] for an oxygen ion distribution of mean energy $\approx$ 100 keV. *Waite et al.* [1983] and *Horanyi et al.* [1988] concluded that electrons and ions give rise to similar effects, but only within about a factor of 2. They also emphasize the significant uncertainty due to the ion cross section estimates, extrapolated at high energy.

Waite et al. [1988] have derived the intensity expected from the sulfur and oxygen lines excitation. The predicted emissions could not be detected with IUE. However, the energy of the incident particles assumed in the model was significantly smaller than the value derived later by *Waite and Boice* [1992], and this can explain the non detection. On the other hand, following *Yung et al.* [1982], *Gladstone and Skinner* [1989] and *Livengood and Moos* [1990] have analyzed the effect of the wavelength dependent atmospheric extinction (due to the hydrocarbons near or below the homopause) on the observed H_2 spectrum. The comparison of the Lyman to Werner band intensity can provide an estimate of the hydrocarbon optical depth above the emitting layer, and given an atmospheric model, the penetration depth of the primary particles. Assuming these particles are electrons, protons, or ions, their energy can be derived (about 10-100 keV, 250 keV-3 MeV, and 100 keV/nucl. - 6 MeV/nucl., respectively). But this method cannot determine the nature of the particles.

An attempt to get simultaneous information on the nature and energy of the precipitating particles is to study simultaneously the ratio of the observed intensity of the H_2 Lyman to Werner bands (only dependent on the energy) and of the H Lyman α line to H_2 bands, which depends on the energy and on the primary species. This has not been systematically studied so far, probably due to the very complex problem of the multiple scattering of the Lyman α photons.

The final goal of this work is to provide the theoretical tool for such a study. The first step of the study, which is presented in this paper, is to get the altitude distribution of the volume excitation rate for the H Lyman α and the H_2 bands for protons and electrons in the energy range which has been suggested by the

spectroscopic results of *Gladstone and Skinner* [1989] and *Livengood and Moos* [1990]: the decay of a proton beam in the Jovian atmosphere has never been specifically studied, and the energy range for electrons has to be extended up to the 10-100 keV range suggested by the latter studies. The ions will not be considered in this first step, although *Waite et al.* [1988] only considered energies well below the *Gladstone and Skinner* [1989], *Livengood and Moos* [1990] and *Waite and Boice* [1992] determinations (≈ 500 keV to several Mev/nucleon), because, as stated by the authors, extrapolating the laboratory data to sill higher energy would not be meaningful. The next step, already in progress, is to develop a radiative transfer code adapted to the transport of the auroral Lyman α photons, in order to model the observed Lyman α / H_2 bands intensity ratio.

In section 2, we establish theoretical expressions for the calculation of the excitation rate, including excitation by the primary beam (protons and/or fast neutral hydrogen from charge transfer) and secondary electrons. The composition of the H/H^+ beam as a function of altitude is studied in section 3, including a discussion of the equilibrium fraction assumption as a function of initial energy. The cross sections used for the various excitation channels and their extrapolation to the convenient energy range when necessary are detailed in section 4. The altitude distribution of the volume excitaton rate for H Lyman α and for the H_2 bands is presented in section 5, discussed as a function of the energy, and compared to the case of electron primaries.

2. Modeling Excitation by Proton Precipitation

2.1. Atmospheric Model

Following *Gérard and Singh* [1982], the total density level $5x10^{13}$ cm^{-3} is defined as reference zero altitude (corresponding to a pressure of about 1 μbar). The precipitating particles are followed from 2000 km, considered as the top of the atmosphere, down to the level of total energy degradation, which occurs, depending on the initial energy of the particles, between ±100 km. Below the altitude 1000 km, the Jovian neutral atmosphere is represented by a recent photochemical model based on the analysis of the Voyager data and modeling of the photochemical reactions and transport of the species [*J. McConnell*, private communication, 1992]. In the model, the input flux of atomic hydrogen has been set to 10^9 cm^{-2} s^{-1}, the eddy diffusion coefficient $K_H = 10^6$ cm^2 s^{-1} (constant with altitude), and an exospheric temperature of 1400 K is adopted (Figure 1). This model is consistent with the Voyager observations and is not representative of an auroral atmosphere (except the exospheric temperature, which has been slightly increased with respect to the value generally used at low latitude, ≈1000 K). Earlier attempts have been made to account for some of the anticipated effects of energetic particle precipitation on the atmosphere itself, such as the use of an increased eddy diffusion coefficient raising the hydrocarbon layers to higher altitude ("polar model" in *Livengood and Moos* [1990]) or the iterative computation of the atomic hydrogen distribution due to ion-neutral reactions above the homopause ("converged model" under electron bombardment of *Waite et al.* [1983]). However, additional effects can be anticipated, such as heating (especially deep in the atmosphere), ion-neutral chemistry under particle bombardment involving the hydrocarbons [*Kostiuk et al.*, 1987; *Halthore et al.*, 1988; *Gladstone and Skinner*, 1989], which have not been consistently modeled so far. More recently, *Kim et al.* [1992] have introduced some temperature increase in the upper atmosphere, and consistently modeled the hydrogen ion-neutral chemistry under 10-keV electron bombardment, but the effect on the hydrocarbons is still neglected.

We thus adopt a classical photochemical atmospheric model with increased exospheric temperature and increased atomic

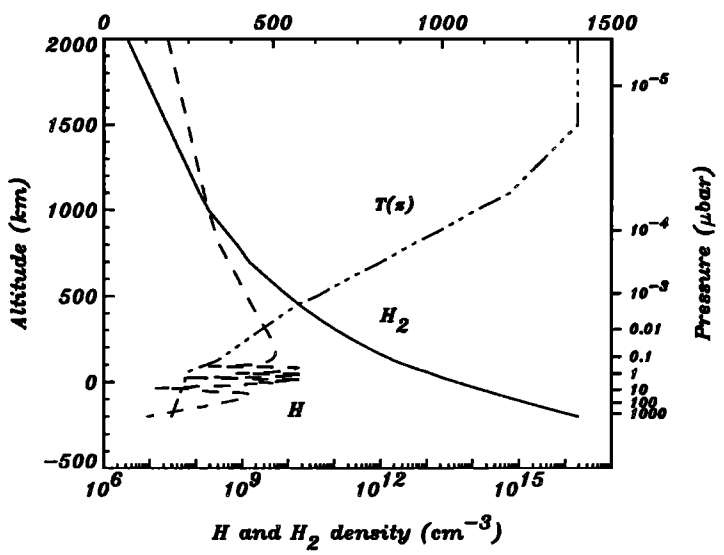

Figure 1. Atmospheric model used. The $n = 5 \times 10^{13}$ cm^{-3} level has been taken as the origin of altitude as in *Gérard and Singh* [1982]. For clarity, the pressure scale is also plotted on the right. Temperature distribution is derived from the Voyager IRIS and UVS observations, except for an increased exospheric temperature assigned to auroral heating. Concerning the altitude distribution of H and H_2 (J. McConnell, private communication, 1992), this model is a photochemical model, normally appropriate to low-latitude regions, except for the increased exospheric temperature. The structure of the H distribution in layers between a few μbar and 0.1 μbar is due to three-body destructive reaction of H with hydrocarbon constituents which are strongly confined in thin layers, and only the average profile will actually be significant for the purpose of our study.

hydrogen input flux as a first approach to construct our excitation rate model (Figure 1). In addition, such a model allows comparison of our results for proton excitation with other previous studies of excitation by electron precipitation made with the same kind of atmospheric model. Above 1000 km, the *McConnell* atmospheric profile is extrapolated upwards by the *Gérard and Singh* [1982] model, based on the *Festou et al.* [1981] analysis of the Voyager occultation data, and using a high 1400 K exospheric temperature to account for auroral heating. Note that the *Gérard and Singh* [1982] model only takes into account the diffusive equilibrium of the hydrogen species, and does not introduce the three-body photochemical reactions which control the atomic hydrogen distribution below the homopause. Therefore, it is not suited to study the deep penetration of very energetic particles such as those which are expected in the Jovian aurora [*Gladstone and Skinner*, 1989; *Livengood and Moos*, 1990].

2.2. Excitation and Ionization by the Primary Particles

The method adopted in this model is based upon the continuous slow down approximation (CSDA). It has been already developped by several authors [*Edgar et al.*, 1973; *Heaps et al.*, 1975; *Edgar et al.*, 1975); *Gérard and Singh* , 1982] and will not be detailed here. This approximation assumes that the loss of energy can be represented by a continuous rather than a discrete loss function. This assumption is reasonable for the high-energy particles which are essentially considered in this study.

The total volume excitation rate is computed in three steps. First, we determine the volume ionization rate of H and H_2 due to the interaction of the primary beam with the atmosphere. We then derive the volume excitation rate for any given line, directly due to these primary particles, and finally, we estimate the contribution of the secondary electrons, produced by ionization of the atmospheric constituents, to the total volume excitation rate.

The number of electron-ion pairs created in a gas s at altitude z per unit time and per unit volume is given by

$$V_s(z)=\frac{1}{\Delta E_s}\int_0^{\infty}\Phi(E_0)dE_0\int_{\Omega}\left[-\frac{dE}{dx}\right]_s f(\theta)d\Omega \qquad (1)$$

where ΔE_s is the average energy expanded in creating an electron-ion pair (= 37eV) in H_2, $\Phi(E_0)$ is the initial differential flux of protons (protons.cm^{-2} s^{-1} eV^{-1}), $f(\theta)$ is the angular distribution of the protons injected at the top of the atmosphere, θ is the angle between the velocity vector of the protons and the local vertical, and $[dE/dx]_s$ is the stopping power of the beam in gas s (eV cm^{-1}).

We assume that θ is constant throughout the process of energy degradation. In particular, we neglect the angular scattering during the collisions, which is an acceptable assumption for energetic particles, any variation of the particle direction due to the effect of the varying magnetic field strength (we have checked that the conservation of the first adiabatic invariant generally does not significantly modify the angular distribution of a beam over the ≈2000 km altitude range if $\theta < 85°$), as well as the effect of the many charge-exchange collisions with the ambient hydrogen which makes the proton spend part of its time as a fast neutral atom and results in a broadening of the beam (the neutral atoms do not follow the field lines) and a corresponding attenuation of the precipitating flux Φ_0. As derived from section 3, the fraction of H remains negligible in the beam for energy greater than 100 keV (less than 15%). The spreading of the beam can therefore be confidently neglected. At lower energy, H may dominate the composition of the beam. We have made a crude estimation of the spreading of the beam by calculating the path traveled by a neutral atom before its first collision. We found that the spreading is approximately 1500 km. A better estimation requires more accurate calculations, but this is not the purpose of this paper.

The stopping power of the beam in the gas s can be expressed by

$$\left[-\frac{dE}{dz}\right]_s=-\frac{n_s(z)}{\cos(\theta)}L_s(E) \qquad (2)$$

where $L_s(E)$ is the loss function of the beam in the gas s and $n_s(z)$ is the density of the gas s.

Equation (2) is then integrated and inverted in order to obtain $E_{loc}(\theta,h)$, which is the local energy, i.e., the beam energy at the altitude h and for the angle θ (see appendix).We choose for the initial differential flux of protons a Maxwellian distribution, i.e.

$$\Phi(E_0)=\Phi_0\frac{E_0}{\alpha^2}e^{-E_0/\alpha}\quad \text{protons.cm}^{-2}\,\text{s}^{-1}\,\text{eV}^{-1} \qquad (3)$$

where α determines the hardness of the spectrum. The mean energy of the beam is 2α.

In addition, and in contrast to previous studies, we introduce an adjustable angular distribution, in order to simulate the possible range of actual distributions of high-latitude precipitating particles. Approximating the high-latitude magnetic field lines by the local vertical, we use the pitch angle (relative to the field direction) instead of θ. *Prangé and Elkhamsi* [1991] represented a wide variety of possible equatorial pitch angle distributions by the simple function $f(\theta)=A_n\sin^n(\theta)$, $f(\theta)$ being the differential angular distribution and n a parameter representative of the anisotropy (n=0 is an isotropic equatorial distribution). The normalization parameter A_n is given by

$$A_{2n}=\frac{2}{\pi}\frac{(2n)!!}{(2n-1)!!}$$
$$A_{2n+1}=\frac{(2n+1)!!}{(2n)!!} \qquad (4)$$

In this paper, we have generally used the isotropic distribution in the equatorial plane (n=0) with qualitative estimates of the effect of different distributions. The effect of anisotropic distributions on the excitation rates profiles is detailed by *R. Prangé et al.* (Auroral Lyman α and H_2 bands from the giant planets, 2, Effects of the anisotropy of the precipitating particles on the interpretation of the 'color ratio', submitted to *Journal of Geophysical Research*, 1994).

We can now estimate the volume ionization rate combining (1) with (2), i.e.,

$$V_s(z)=\frac{2\pi n_s(z)}{\Delta E_s}\int_0^{\infty}\Phi(E_0)dE_0\int_0^{\pi/2}L_s(E_{loc})f(\theta)\tan(\theta)d\theta \qquad (5)$$

The volume excitation rate of the state i at the altitude z due to the interaction of the beam with the gas s is

$$V_{i,s}(z)=2\pi n_s(z)\int_{E_0}\int_{\theta}\frac{dJ_i}{dE}(E_{loc})\,\Phi(E_0)\,L_s(E_{loc})f(\theta)\tan(\theta)d\theta\,dE_0 \qquad (6)$$

where $J_i(E_{loc})$ is the population of the state i of the specie s. Due to charge exchange collisions with the atmosphere, the protons in the incident beam are rapidly replaced by a mixture of protons and fast H atoms (H_f). If $F_0^s(E)$ and $F_1^s(E)$ are the energy dependent

fractions of H_f and protons of a beam penetrating in the gas s (evaluated in section 3) respectively, $J_i(E_{loc})$ can be expressed as the sum of the H_f and proton contributions:

$$J_i(E_{loc}) = J_{i,H}(E_{loc}) + J_{i,p}(E_{loc}) \quad (7)$$

where

$$J_{i,H}(E_{loc}) = \int_{E_i^{th}}^{E_{loc}} \frac{F_0^s(E)\sigma_{i,H}(E)}{L_s(E)} dE \quad (8a)$$

$$J_{i,p}(E_{loc}) = \int_{E_i^{th}}^{E_{loc}} \frac{F_1^s(E)\sigma_{i,p}(E)}{L_s(E)} dE \quad (8b)$$

where $\sigma_{i,H}$ and $\sigma_{i,p}$ are the energy dependent excitation cross sections of the state i due to H_f and proton impact respectively. E_i^{th} is the energy threshold of the reaction. Combining equations (8.a) and (8.b) with equation (6), we obtain

$$V_{i,s}(z) = 2\pi n_s(z) \int_{E_0}\int_{\theta} \left[F_1^s(E_{loc})\sigma_{i,p}(E_{loc}) + F_0^s(E_{loc})\sigma_{i,H}(E_{loc})\right] \times \Phi(E_0) f(\theta) \tan(\theta) d\theta \, dE_0 \quad (9)$$

The total volume excitation rate of the state i due to the interaction of the beam with the Jovian atmosphere is the sum of the volume excitation rate for H and H_2 if both produce the excited state i. This is the case for the H($2p$) state which produces H Lyman α.

2.3. Excitation by the Secondary Electrons

Secondary electrons are produced by ionization of H and H_2 by the H^+/H_f beam. They can interact with the atmospheric constituents and excite them. We will not consider the effect of tertiary electrons produced by ionization of H and H_2 by secondary electrons, since the volume ionization rate due to the secondary electrons is several orders of magnitude smaller than the volume ionization rate due to the beam (Figures 2a and 2b). We have checked this result for several initial energies.

According to the expression given by *Gérard and Singh* [1982] for the secondary electron production rate $\eta_s(E_{sec},z)$, we have for the gas s,

$$\eta_s(E_{sec},z) = \frac{2\pi n_s(z)}{\Delta E_s} \int_{E_0} \Phi(E_0) dE_0 \times \int_{\theta} L_s(E_{loc}) f(\theta) \tan(\theta) S_s(E_{sec},E_0) d\theta \quad (10)$$

where E_{sec} is the ejected electron energy and $S_s(E_{sec},E_0)$ is the "shape parameter". This quantity is defined by

$$S_s(E_{sec},E_0) = \frac{\sigma_{ion}(E_{sec},E_0)}{\sigma_{ion}(E_0)} \quad (11)$$

where $\sigma_{ion}(E_{sec},E_0)$ is the differential cross section for the production of an electron with energy E_{sec} through ionization of s by a proton of energy E_0 and $\sigma_{ion}(E_0)$ is the total ionization cross section of s by proton impact. In the case of primary electron precipitation and according to the results of *Opal et al.* [1971], the "shape parameter" is independent of the primary energy above 300 eV. By contrast, in the case of H^+/H_f precipitation, the "shape parameter" depends on the primary energy. From the work of *Rudd* [1979], we deduce the following expression for the "shape parameter" of protons in H_2 :

$$S_{H_2}(E_{sec},E_0) = \frac{a}{\sqrt{IT}} e^{-aE_{sec}/\sqrt{IT}} \quad (12)$$

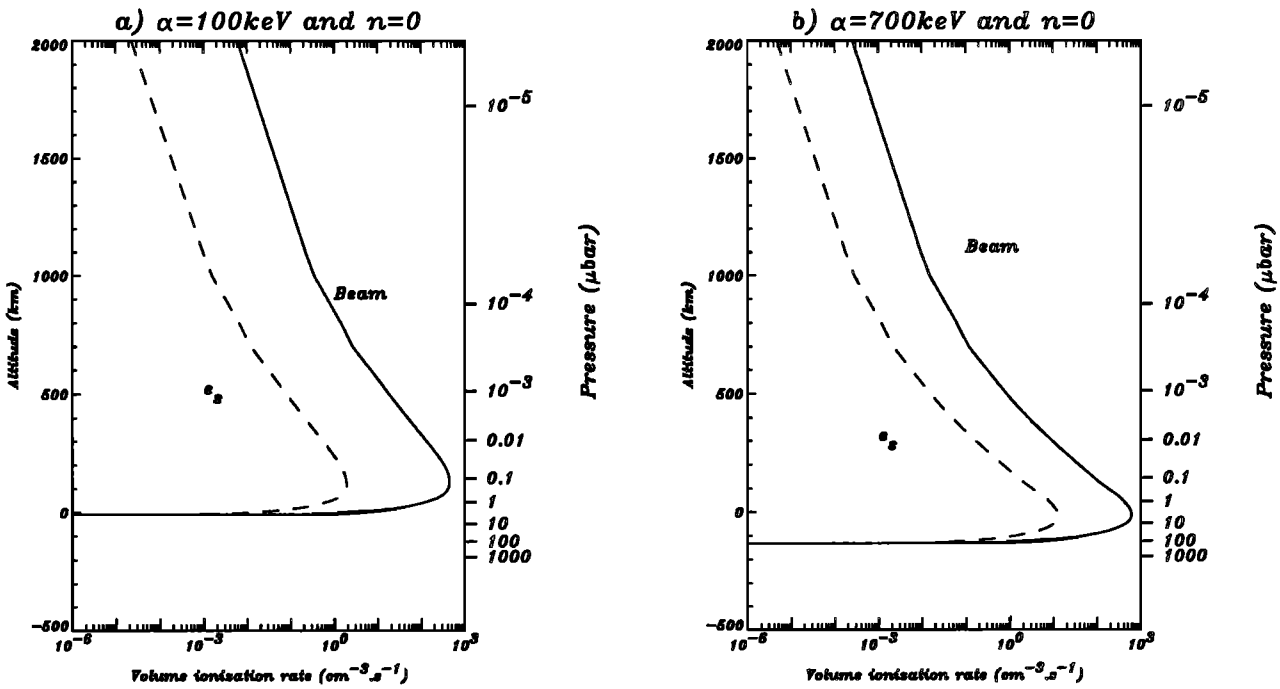

Figure 2. Altitude distribution of the volume ionization rate due to the particles in the precipitating beam (protons, H^+, and fast neutral hydrogen H_f), and the secondary electrons for initial energies of the beam of 100 and 700 keV. The angular distribution used corresponds to n = 0 (see text). The ionization from the secondary electrons is several orders of magnitude smaller than that from the beam particles (for the two energies considered), so that tertiary electrons can be neglected.

where a = 1.28 (dimensionless constant for H_2), I = 15.4 eV, and $T = E_0/1836$.

A similar calculation is made for the production rate of the secondary electrons from H, assuming a similar "shape parameter". Then, according to the expression given by *Rees et al.* [1969], the differential flux of secondary electrons at the altitude z for the energy E_{sec} is

$$\Phi_{sec}(E_{sec},z)=\frac{\int_{I_{H_2}}^{E_{sec}}\eta_{H_2}(E,z)\,dE+\int_{I_H}^{E_{sec}}\eta_H(E,z)\,dE}{[-dE/dx]_{e-H_2}+[-dE/dx]_{e-H}+[-dE/dx]_{e-e}} \quad (13)$$

where $[-dE/dx]_{e\text{-}H_2}$ and $[-dE/dx]_{e\text{-}H}$ are the stopping power of electrons in H_2 and H, respectively [*Cravens et al.*, 1975; *Gérard and Singh*, 1982]. For the stopping power of electrons with thermal electrons, we use the expression of *Swartz et al.* [1971], i.e.,

$$\left[-\frac{dE}{dx}\right]_{e-e}=\frac{3.37\times10^{-12}[n_e(z)]^{0.97}}{(E_{sec})^{0.94}} \quad (14)$$

where $n_e(z)$ is the altitude dependent electronic density.

Assuming that the secondary electrons are degraded locally, the expression for the volume ionization rate due to the secondary electrons is

$$V_{s,sec}(z)=n_s(z)\int_{E_i^{th}}^{\infty}\Phi_{sec}(E_{sec},z)\sigma_{ion,s}(E_{sec})dE_{sec} \quad (15)$$

where $\sigma_{ion,s}$ is the differential ionization cross section of the gas s by electron impact. Values calculated by *Green and Sawada* [1972] for the ionization of H_2 are adopted. For electron impact on H, the cross section of *Janev et al.* [1987] is used.

For the volume excitation rate of the state i of s due to secondary electrons at altitude z, we have

$$V_{i,s}(z)=n_s(z)\int_{E_i^{th}}^{\infty}\Phi_{sec}(E_{sec},z)\sigma_{i,s}(E_{sec})dE_{sec} \quad (16)$$

where $\sigma_{i,s}$ is the excitation cross section of the state i by electron impact on s. For the production of excited H(n) with n=2-6 by electron impact on H, cross sections of *Olivero et al.* [1973] are adopted. In H_2, data of *Ajello et al.* [1991] for H Ly α production cross section and analytical expression of *Garvey et al.* [1977] for the H_2 bands (Lyman and Werner bands) production are adopted. The total volume excitation rate of this state due to the secondary electron is the sum of equation (16) for H and H_2 if both produce the excited state of interest.

Finally, the total volume excitation rate of the state i is the sum of equation (6) and equation (16) for all the atmospheric constituents which produce the excited state i.

3. Effect of Charge-Exchange on the Precipitating Beam Composition

As previously mentioned, part of the collisions of the protons with the atmosphere takes place in the form of charge transfer interaction, without any momentum transfer. This results in the creation of fast neutral atomic hydrogen through reversible reactions.

The precipitating H_f in the beam also contributes in the H_2 bands and H Ly α excitation. Consequently, the fractions of H_f and protons in the beam must first be determined in order to estimate their contributions to the excitation.

3.1. Determination of Beam Equilibrium Fraction: Altitude Dependence

The formalism of charge-exchange has been reviewed by *Allison* [1958] and only the results will be reported here. Provided the atmospheric column density along the particle path is sufficient, the beam can reach its equilibrium composition. This is the assumption which is usually made.

The equilibrium fractions of H_f and protons, noted by F_0^s and F_1^s, respectively, for a pure proton beam penetrating in a gas s, are given by

$$F_0^s=\frac{\sigma_{10}}{\sigma_{01}+\sigma_{10}} \qquad F_1^s=\frac{\sigma_{01}}{\sigma_{01}+\sigma_{10}} \quad (17)$$

where σ_{10} and σ_{01} are the energy dependent electron capture and ionization stripping cross sections for the gas s (according to *Allison* [1958], we neglect the presence of H^-, since its equilibrium fraction in H_2 is smaller than 2% for all energies of the beam). In H_2, analytical expressions of *Green and McNeal* [1971] for σ_{10} and σ_{01} have been adopted and in H, the analytical form of *Janev et al.* [1987] for σ_{10} is used. For σ_{01} in H, the data of *Gealy and Van Zyl* [1987a,b] are used for a beam energy between 100 eV and 20 keV, and for higher energies, results by *McClure* [1968] are adopted. Equation (17) shows that the equilibrium fractions are energy-dependent. Moreover, during the decay of the H^+/H_f beam, its energy changes and is a function of altitude and pitch angle. Thus the equilibrium fractions F_0^s and F_1^s are altitude and pitch angle dependent.

In fact, equation (17) is given for a single gas, whereas the Jovian upper atmosphere is primarily a mixture of H and H_2, with respective fractional abundance $f_H(z)$ and $f_{H_2}(z)$. Consequently, the effective equilibrium fractions at a given altitude z are given by the following expressions:

$$F_0(E,z)=f_H(z)F_0^H(E)+f_{H_2}(z)F_0^{H_2}(E) \quad (18a)$$

$$F_1(E,z)=f_H(z)F_1^H(E)+f_{H_2}(z)F_1^{H_2}(E) \quad (18b)$$

The proton and H_f equilibrium fractions in the beam are related by

$$F_1^s(E_{loc})=1-F_0^s(E_{loc}) \quad (19)$$

Once $E_{loc}(z)$ is determined (appendix), we can estimate $F_0^s(E_{loc})$, which gives the altitude dependence of the equilibrium fraction of H_f in the gas s.

The contributions from H and H_2 to the effective proton equilibrium fraction (right-hand terms in equation (18b)) are plotted in Figure 3 versus altitude for several values of the incident proton energy. Due to the fact that the local energy depends on the pitch angle, we have to specify this latter value. For demonstration purposes, we have only considered the limiting case of field-aligned precipitating protons. The effect can be qualitatively derived for other pitch angles. We first plot the equilibrium fraction of H^+ in H and H_2. It is roughly constant over a large range of altitudes, down to a given level (≈500 km for 10-keV incident protons, decreasing with increasing initial energy), due to the fact that the energy loss of the particle is small, and the local energy almost constant and equal to the initial energy. The fraction of H^+ increases with incident energy, both in H and in H_2

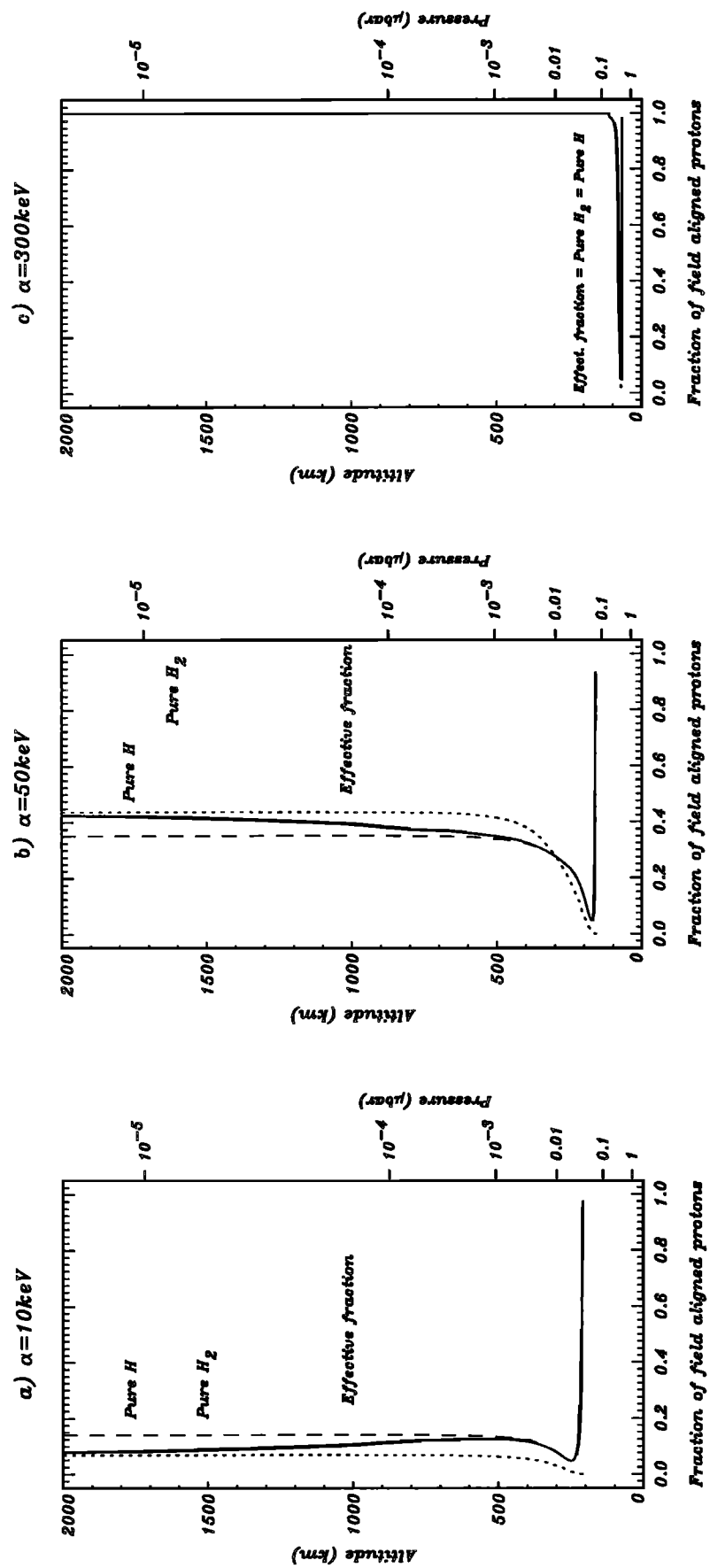

Figure 3. Equilibrium fraction of protons in a precipitating beam as a function of altitude, and for various incident energies. The dotted lines represent the equilibrium fraction on a single specie atmosphere (pure H or pure H_2), and the solid line the equilibrium fraction in the model atmosphere. We have used a field-aligned beam. It is clear that for the range of energies of interest in this paper, the beam is dominated by H^+ at equilibrium, except in a very thin layer, close to the total energy degradation level, where H_2 dominates. However, this is not the case at lower energies.

(≤20% at 10 keV, ≈45% at 50 kev, and ≈100% at 300 keV), and it is always smaller in H than in H_2 for energies larger than 30 keV, although the difference is decreasing with increasing initial energy and vanishes for $E_0 \approx 300$ keV (where it reaches 100% in both cases). Below this particular level where the local energy starts to be significantly smaller than the incident energy, the H^+ fraction decreases to a very low value in all cases. The beam tends toward almost pure H_f just above the level of total energy degradation. We also plot the effective H^+ equilibrium fraction in the actual atmosphere, derived from equation (18b). We note that the major constituent controls the value of the equilibrium fraction which is no longer constant with altitude. At the top of the atmosphere, the equilibrium fraction is that of an approximatively pure H atmosphere, and as the altitude decreases, $F_1(E_{loc})$ decreases so as to merge the pure H_2 atmosphere curve when H_2 dominates the atmospheric composition. At 300 keV and at any higher energy, the presence of atomic hydrogen in the atmosphere does not play any significant role in the calculation of the equilibrium fractions, since the values of the fractions in H and H_2 are very close, but for lower energies, the composition of the beam does not only depend on the initial energy, but also on the composition of the model atmosphere used.

For different angular distributions, the particle path length to a given altitude is increased as $(\cos\theta)^{-1}$. Consequently, the local energy decreases faster, and the equilibrium is displaced toward H_f at higher altitude.

3.2 Equilibration of the Beam: Nonequilibrium Fractions

The usual assumption that the beam's composition is everywhere at equilibrium value is implicitly based on the assumption that the atmosphere is sufficiently dense to equilibrate the beam locally. In fact, the precipitating particles penetrate the atmosphere from the top downwards, and the gas is very tenuous at the beginning. One can therefore question the validity of the assumption of 'instantaneous' equilibrium.

In order to check this assumption, we consider the expressions for $F_0(E_{loc})$ in the nonequilibrium case [*Allison*, 1958] :

$$F_0 = F_{0\infty}\left\{1 - e^{-\pi(\sigma_{01}+\sigma_{10})}\right\} \qquad (20)$$

$$F_1 = 1 - F_0$$

where $F_{0\infty}$ is the equilibrium fraction of H_f (see equation (17)), σ_{01} and σ_{10} are the energy-dependent electron capture and ionization stripping cross sections in cm^2, and π is the column density in cm^{-2}.

Expressions similar to equation (18) can be written for the case of a mixture of gases.

As the beam penetrates into the atmosphere, F_0 approaches the equilibrium fraction $F_{0\infty}$, but the equilibrium fraction of protons is always an underestimate of the actual proton fraction. The difference depends on the value of the exponential term, and one can see that the column density needed to make it negligible varies as the inverse of the cross sections. These cross sections maximize in the range 1-30 keV. Consequently, the altitude where equilibrium is reached decreases with the incident energy from 10 keV to 300 keV (Figure 4). However, in the case of 300 keV (and in fact above 200 keV), the equilibrium fraction (≈100% H^+) is identical to the initial composition of the beam, i.e., for initial energies greater than 200 keV, the beam is already equilibrated at the top of the atmosphere (it would be quite different in the case of a beam of incident neutrals). This gives evidence that at low energy (less than 10 keV) and at high energy (≥200 keV), the beam composition is always equilibrated in the altitude range of the peak excitation rate, although for different physical reasons. However, for intermediate energies, the beam equilibrium composition is reached in a region where the excitation rate is within 1 order of magnitude of its peak value (Figure 5). Considering the fact that emission excited at the peak of excitation contributes less to the observed emission than emission excited above, due to the effect of atmospheric extinction, the problem of equilibration of the beam must be considered carefully in this intermediate energy range, $50 \le E < 200$ keV. The change in composition of the beam at the bottom of the atmosphere is not affected by this problem, since the atmosphere there is dense enough to insure instantaneous equilibration. We have also investigated the effect of the pitch angle on the equilibration of the beam. When the pitch angle increases (increasing the path of the particles), the point where the equilibrium is reached is displaced upward. At this point, the excitation rate is still important in comparison to the value at the peak. For pitch angles greater than 80°, the path length is sufficiently large that it allows the equilibration of the beam in the very upper atmosphere. Then the entire region contributing significantly to the excitation rate is traversed through an equilibrated beam.

Finally, as mentioned above, the volume excitation rates present a peak which corresponds to the region where the local energy E_{loc} rapidly decreases. In this region, only a few hundred kilometers thick, it is important to know which precipitating particles will be dominating the excitation process. We plot in Figure 5, the contribution of protons and fast hydrogens to the excitation rate of the H_2 Lyman bands for three different incident energies, and show that three different kinds of situations must be distinguished. In the altitude range of the peak, the excitation process will be controled by H_f impact ($E < 2$-10 keV), by a mixture of H_f and protons (2-10 keV $< E < 200$ keV) or by proton impact ($E > 200$ keV). The energy ranges are, of course, approximate estimates of the limits of the different situations.

Based on these results, it is clear that there are two relatively simple situations: low-energy precipitating proton beams (a few keV) and high-energy precipitating proton beams (> 200 keV), where the equilibrium composition is always reached, and where the excitation process is dominated by a single specie (H_f and H^+, respectively). The intermediate situation is more complicated, with a mixture of H_f and H^+ on the whole range of altitude, and for which we must take into account the nonequilibration of the beam.

The specific goal of this first paper is the analysis of the Jovian auroral emissions. As detailed in the introduction, several independent studies have suggested that the precipitating particules should be rather energetic. *Livengood and Moos* [1990] have deduced the penetration depth of the particles from hydrocarbon absorption signatures. They conclude that protons of energy between 250 keV and 1.6 MeV could have such a range in an H_2 atmosphere. The use of a precomputed penetration range table entails the assumption of normal penetration in the atmosphere, i.e., rougly field-aligned distributions. Any other angular distribution would imply larger incident energy. This energy range is also consistent with the determination of ≈700 keV/nucleon for precipitating O and S ions analyzed by *Waite and Boice* [1992]. Consequently, in the following, we will focus on the high-energy case. It is clear that for applications to the other giant planets, the more complex case of intermediate energy protons should be developed also. Therefore, we have also studied the case of 50 keV primary protons for comparison purposes.

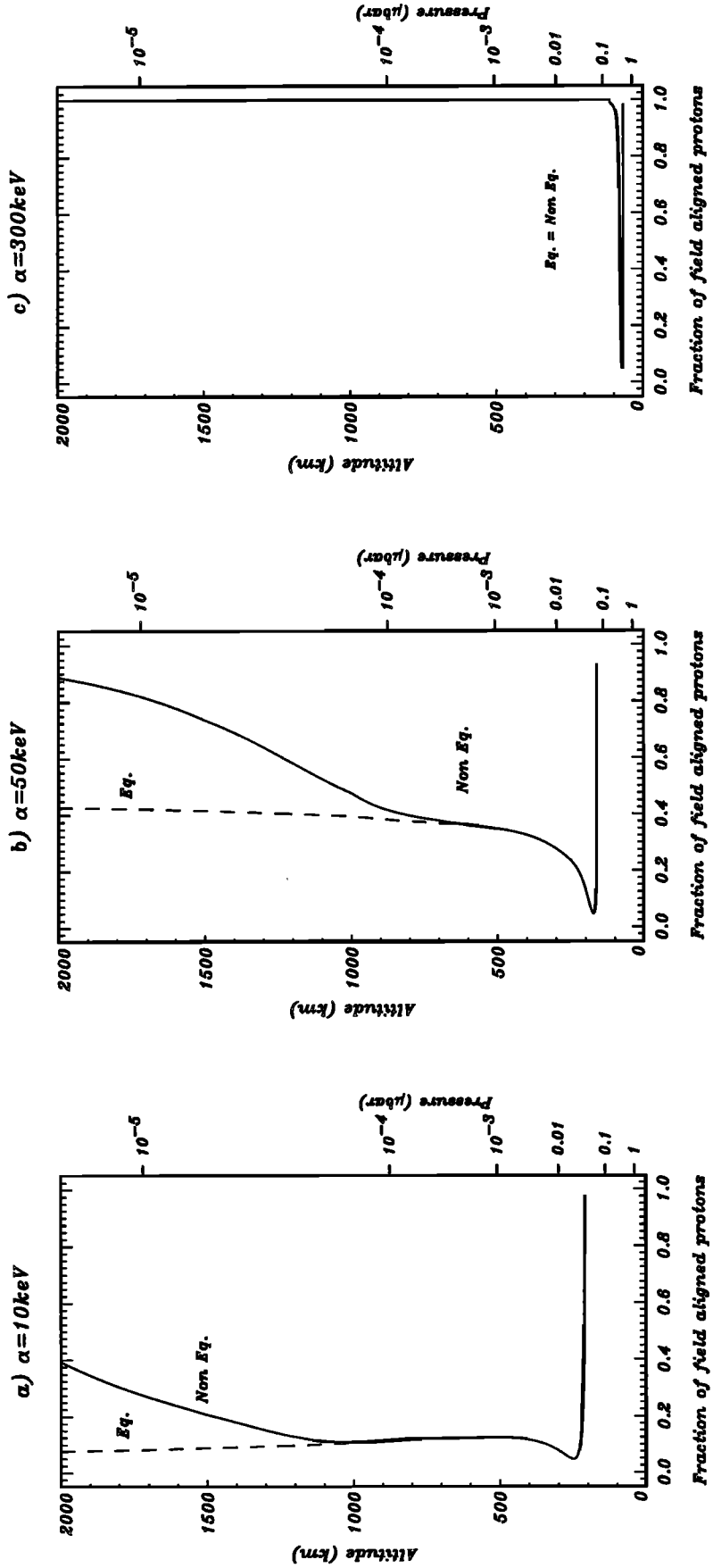

Figure 4. Comparison of the actual (nonequilibrium) beam composition with the result of the assumption of equilibrium composition for various incident proton energies. The fraction of H^+ in the beam is computed for an incident beam of field-aligned protons. Due to a larger ratio of particle path/altitude range, the altitude where equilibrium is reached is larger if the angular distribution is not along the field (but the altitude of total energy deposition and of maximum peak excitation is larger also).

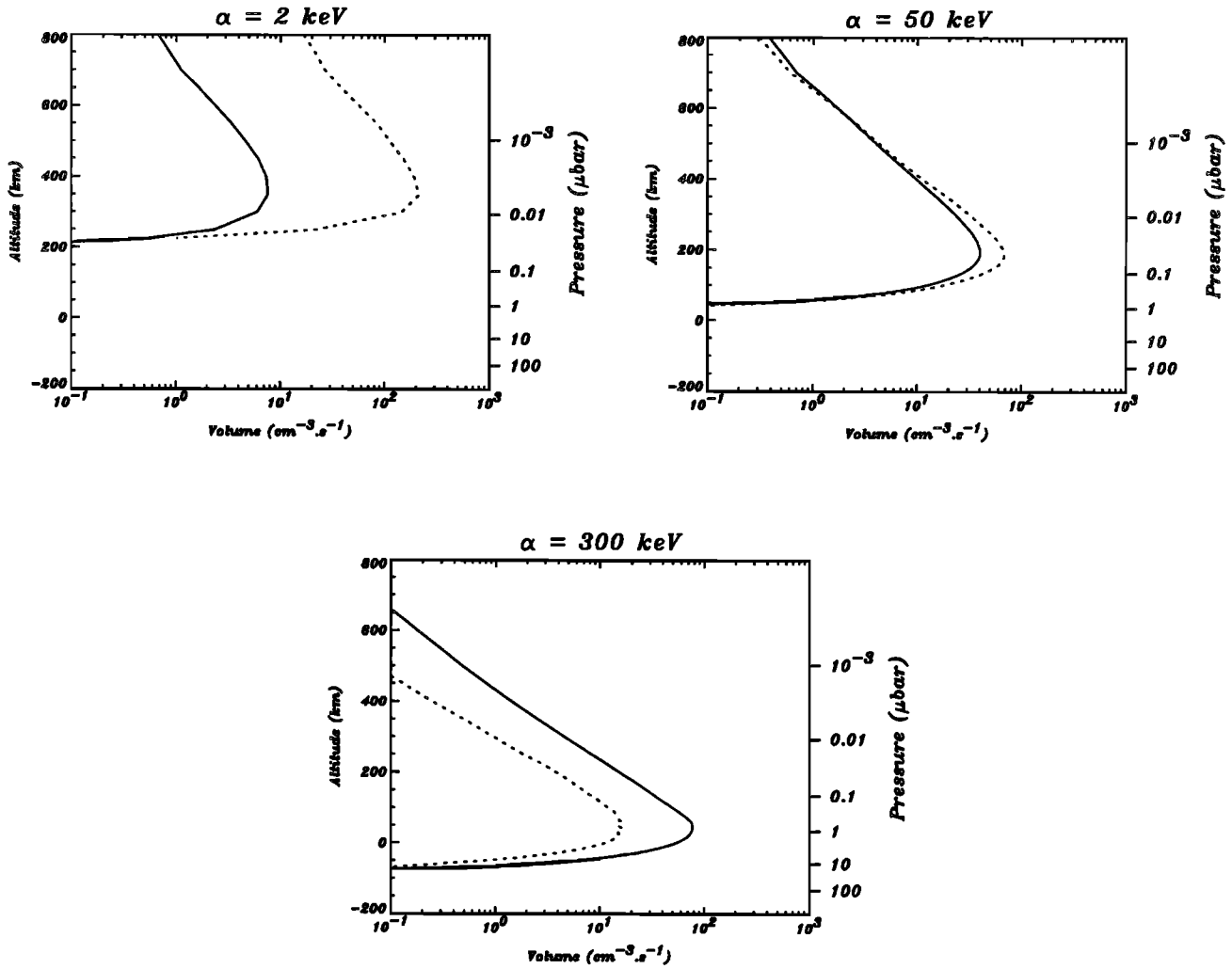

Figure 5. Contribution of the protons and of the fast hydrogen atoms to the volume excitation rate of the Lyman bands for various incident proton energy in the altitude range of the peak. The process is dominated by fast hydrogen for low incident energy, and by protons for high incident energy. At 50 keV, the beam consists of a mixture of H^+ and H_f where one or the other dominates alternately.

4. Excitation Processes and Cross Sections

4.1. Reactions and Cross-Section Data

In order to evaluate the volume excitation rate of H Ly α from the atmospheric constituents H and H_2, we have considered the various processes of production for this emission. They are all presented in the Table 1 with the respective source of data we have used for our code. When no experimental data are available, the cross sections have been extrapolated.

Due to the lack of laboratory measurements for the excitation of H_2 bands by proton and atomic hydrogen impact, we have used scaling laws [*Miller and Green*, 1973] for proton impact. These laws allow the determination of the excitation cross section by proton impact knowing the corresponding cross section due to electron impact. The electron impact excitation cross section used for the Lyman and Werner bands is the analytical form given by *Garvey et al.* [1977]. Concerning the excitation of the H_2 bands by fast hydrogen impact, we have assumed the same ratio between the H Lyman α and H_2 band cross sections for protons and fast H on H_2 (the cross section for production of Lyman α by H_f on H_2 is measured; see the references in Table 1).

4.2. Results

Figure 6 shows the volume ionization rates of the two atmospheric constituents (H and H_2) and the contribution of the secondary electrons (e^-_s) which leads to the formation of tertiary electrons. This latter contribution is several orders of magnitude lower than the beam contribution. However, by comparison with Figure 2, it appears that the contribution of the secondary electrons is slightly increasing with energy (from ≈0.4% to 2.1% of the total number of ionizations from 100 keV to 700 keV). One can also observe that the altitude of the peak ionization rate decreases from ≈130 km to ≈-12 km. In any case, for energetic precipitating protons, ions are preferentially produced by the beam impact on the Jovian atmosphere, and we expect that the contribution of the tertiary electrons to the volume ionization rate is negligible.

Table 1. Cross Sections for H Lyman α Production

Reactions	Energy Range	References
$p + H_2 \rightarrow Ly\,\alpha$	160eV-1keV	*Van Zyl et al.* [1989]
	1keV-40keV	*Birely and McNeal* [1972]
	40keV-100keV	*Hughes et al.* [1972]
	>100keV	extrapolated
$H + H_2 \rightarrow Ly\,\alpha$	50eV- 3keV	*Van Zyl et al.* [1989]
	3keV-20keV	*Birely and McNeal* [1972]
	>20keV	extrapolated
$p + H \rightarrow p + H(2p)$	All energies	*Janev et al.* [1987]
$p + H \rightarrow p + H(2s)$	10.2eV-80keV	*Janev et al.* [1987]
	>80keV	extrapolated
$p + H \rightarrow H(2p) + p$	10.2eV-60keV	*Janev et al.* [1987]
	>60keV	extrapolated
$p + H \rightarrow H(2s) + p$	1keV-100keV	*Morgan et al.* [1980]
	>100keV	extrapolated
$H + H \rightarrow H + H(2p)$	1keV-100keV	*Shingal et al.* [1987]
	>100keV	extrapolated
$H + H \rightarrow H + H(2s)$	1keV-100keV	*Shingal et al.* [1987]
	>100keV	extrapolated
$H + H \rightarrow H(2p) + H$	1keV-40keV	scaling law
	>40keV	extrapolated
$H + H \rightarrow H(2s) + H$	1keV-100keV	*Mayo et al.* [1988]
	>100keV	extrapolated

Figure 7 represents the differential energy spectrum of the secondary electrons, given by equation (14), at various altitude levels between the top of the atmosphere and the level where the incident particles have lost all their energy (≈0 km). We see its deformation as the altitude decreases. The fact that this flux is greater for the low energies is due to the reactions of the secondary electrons with the atmospheric species (ionization or excitation) which all have thresholds near or above 10 eV. This effect increases as the atmosphere becomes denser at lower altitudes, enhancing the low-energy part of the spectrum with respect to the high-energy tail. In addition, thermalization reactions (for example, loss by vibrational excitation of H_2) also redistribute the energy of the secondary electrons toward very low energies. This appears in the relative increase of the spectrum below ≈1-3 eV, increasing with decreasing altitude, and maximum at the lower level reached by the beam (0 km, here).

In Figure 8a, we plot the volume excitation rate of H Lyman α, which is the sum of the excitation coming from the two atmospheric species (H and H_2) which both produce this line. The contributions of the two components of the beam, H^+ and H_f, and of the secondary electrons are separated in order to estimate their relative importance. We note that the main source of excitation comes from e^-_s impact : ≈68% of the total excitation rate at the top of the atmosphere, and 55% at the peak level (45 km). At the peak, excitation by H_f impact is 2.5 times smaller than the excitation by protons, and approximately 13% of the total. As altitude increases, the role of the fast H to the excitation decreases to a negligible level. However, even with a small fraction of fast H in the beam, its contribution at the peak is not negligible. So, with smaller initial energies, we would expect the fast H contribution to increase (Figure 8b).

Figure 9 shows the volume excitation rate of the Lyman and the Werner bands of H_2. Fast H, proton, and secondary electron contributions have been separated. As for H Lyman α, secondary electrons are the main contributor to the excitation of the H_2 bands (≈71% at the peak and 68% at the top of the atmosphere for the Lyman bands, and 71% and 68%, respectively, for the Werner bands). Fast H contributes approximatively 5% of the total excitation rate at the peak. Fast H is more efficient for the excitation of H Lyman α than for the H_2 bands for α = 300 keV.

5. Comparison Between Electron and Proton Precipitations

5.1. The Electron Code

A code for modeling electron precipitation has also been developed. The method adopted in this model is still the CSDA. We will only present here the main results. From *Gérard and Singh* [1982], the number of ion pairs created in a gas s per unit time and per unit volume is similar to equation (1) except that the stopping power is that for electrons in H_2. We use the expression of the loss function $L(E)$ of electrons in H_2 given by *Gérard and Singh* [1982]. The volume ionization rate expression due to electron impact on the atmospheric gas s is the same as equation (6) after replacing the correct loss function $L_s(E)$.

A major simplification arises from the disappearance of the charge exchange process when the incident beam comprises only electrons, and the expressions for the volume excitation rates are somewhat different. We will not explicitly outline the various steps leading to these expressions, for they are similar to the proton case. So, the volume excitation rate of the state i at the altitude z due to the interaction of the electrons with the gas s is

$$V_{i,s}(z) = 2\pi n_s(z) \int_{E_0} \int_{\theta} \sigma_{i,e}(E_{loc})\, \Phi(E_0) f(\theta) \tan(\theta)\, d\theta\, dE_0 \quad (21)$$

For the secondary electrons contributions, the production rate expression is similar to equation (10) except for the "shape parameter". It is given by *Opal et al.* [1971] and has the following form:

$$S_{H_2}(E_{sec}, E_p) = \frac{2}{\pi b \left\{1 + \left(E_{sec}/b\right)^2\right\}} \quad (22)$$

where b = 8.3 eV for H_2 and E_p is the primary electron energy. We note that the "shape parameter" is independent of the primary energy above 300 eV.

The differential flux of secondary electrons at the altitude z for the energy E_{sec} is given by equation (13), where the secondary electron production rates are calculated with the new "shape parameter". Assuming a local degradation of the secondary electron energy, the volume ionization and excitation rates due to the secondary electrons are given by equation (15) and equation (16), respectively.

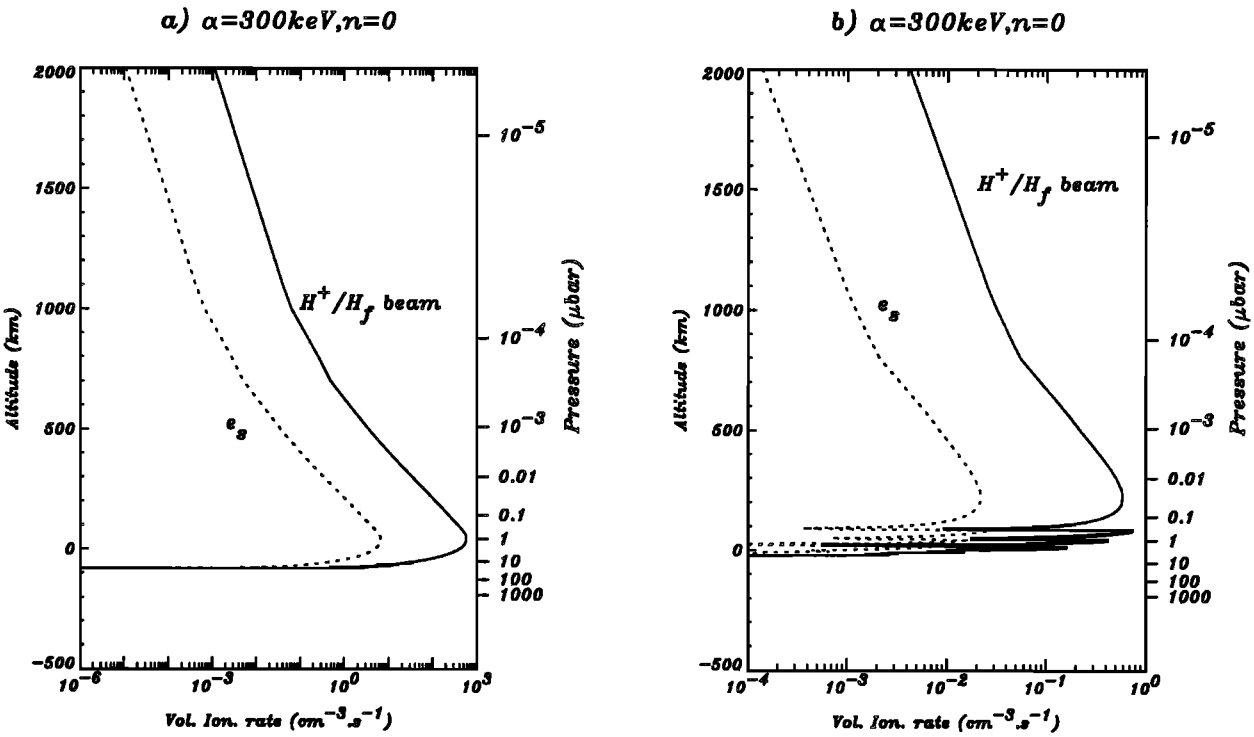

Figure 6. Contribution of the beam particles (H^+ and H_f) and of the secondary electrons to the ionization rate of (a) H_2 and (b) H after determination of the altitude-dependent equilibrium fraction.

As for the proton case, total volume rates are the sum of the primary and the secondary contributions.

In order to compare the effect of the species in the incident beam (electrons or protons), one must cancel any effect due to the initial energy. We have therefore first computed the altitude where the energy of 300 keV incident protons would be totally degraded, and using the electron code, we have determined the beam initial energy that allows electrons to reach the same altitude. The corresponding electron initial energy is 10 keV, computed with field-aligned beams in both cases.

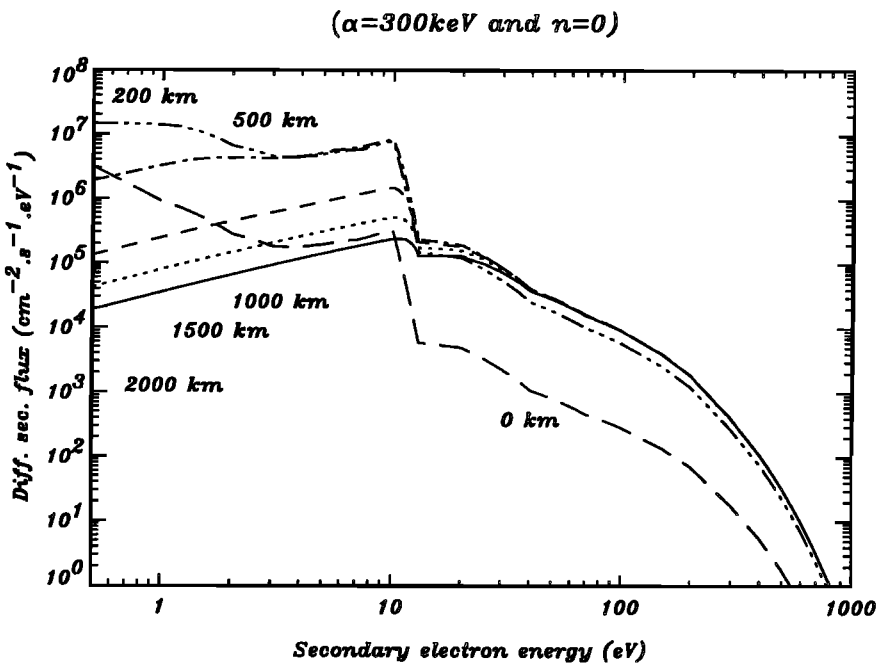

Figure 7. Differential energy spectra of the secondary electrons created by a 300-keV proton incident beam at various altitude levels. One can see that the increased thermalization of the electrons enhances the low-energy population at the expense of the high-energy tail. The maximum overall production is near 100 km (≈ ionization peak in Figure 6), and minimizes at 0 km, which is close to the total energy degradation level for 300 keV at the top of the atmosphere.

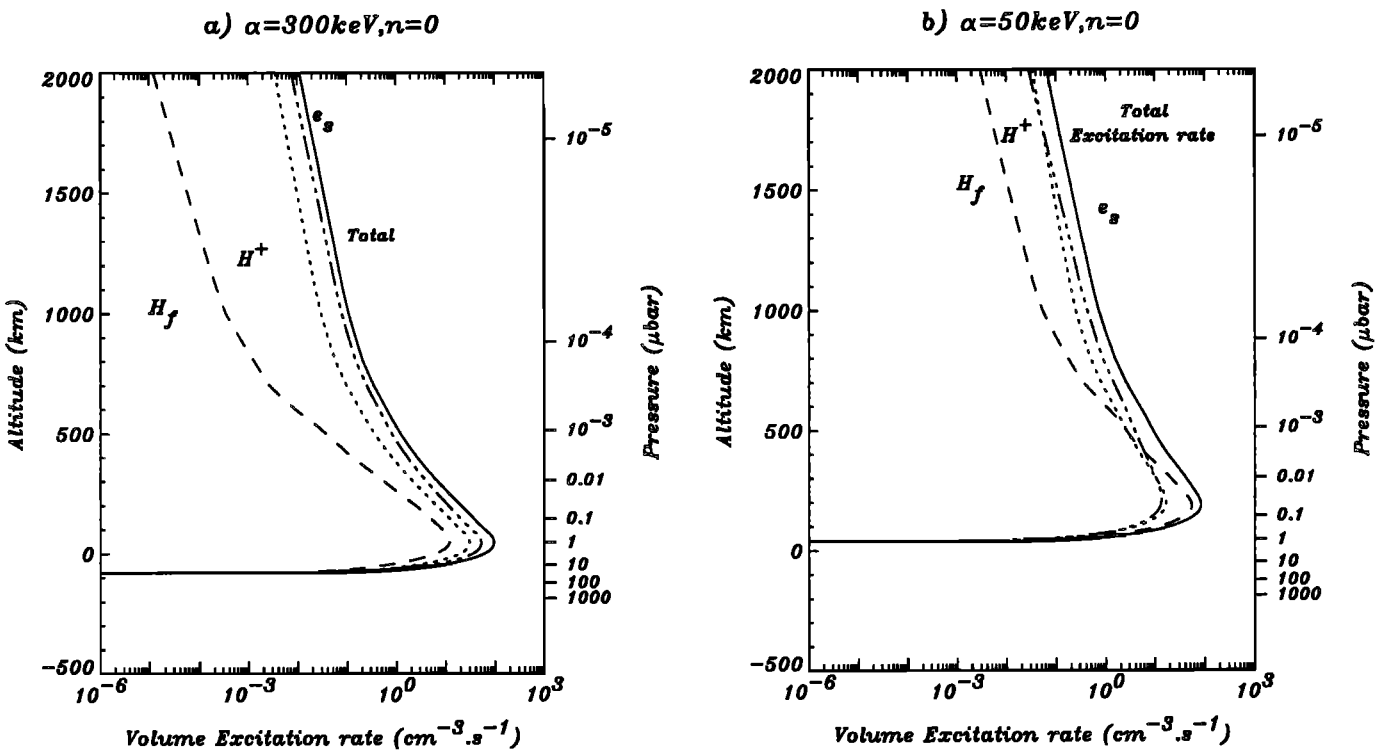

Figure 8. Altitude distribution of the total excitation rate of H Lyman α and of the individual contributions from fast hydrogen H_f, from the protons (H^+) and from the secondary electrons e_s^- for (a) a 300-keV proton incident beam and (b) a 50-keV proton incident beam. The volume excitation rate is dominated by the effect of the secondary electrons for large incident energies (greater than 200 keV) and by the effect of the fast H for small energies (less than 100 keV).

5.2. Comparison of the Ionization and the Excitation Rates due to Proton and Electron Impact

We compare in this section the volume ionization and excitation rates induced by electron and proton precipitation.

Figure 10 shows the altitude distribution of the volume ionization rate of H_2. The 10-keV electrons and the 300-keV protons produce extremely similar effects. In addition to a similar penetration depth (imposed by the choice of the energies), we can note that in both cases, the secondary electron contributions are quite similar (≈1% of the total contribution), and are negligible for the ionization of the atmosphere. In addition, the absolute value of the volume ionization rate is about the same all over the altitude range, except for a relatively small excess of the primary electron ionization with respect to the H^+/H_f beam at the top of the atmosphere (≈1.4 times larger).

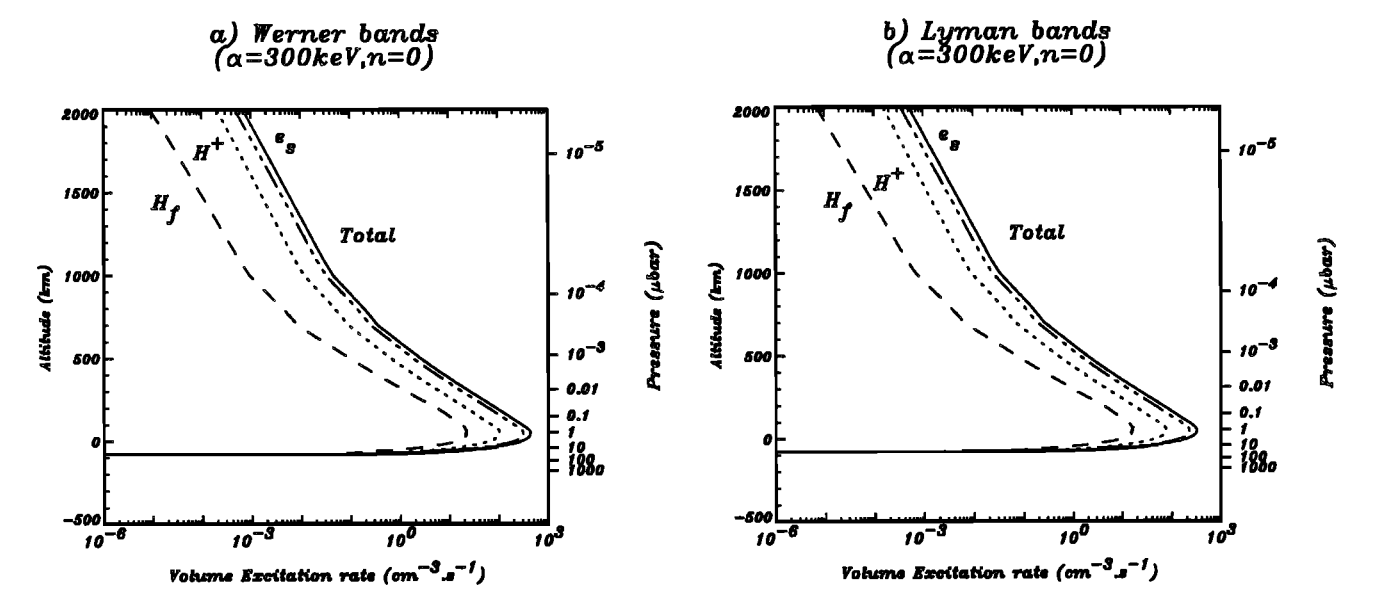

Figure 9. Plots for the (a) Werner bands and (b) the Lyman bands of H_2. Again, the excitation rate is dominated by the effect of the secondary electrons.

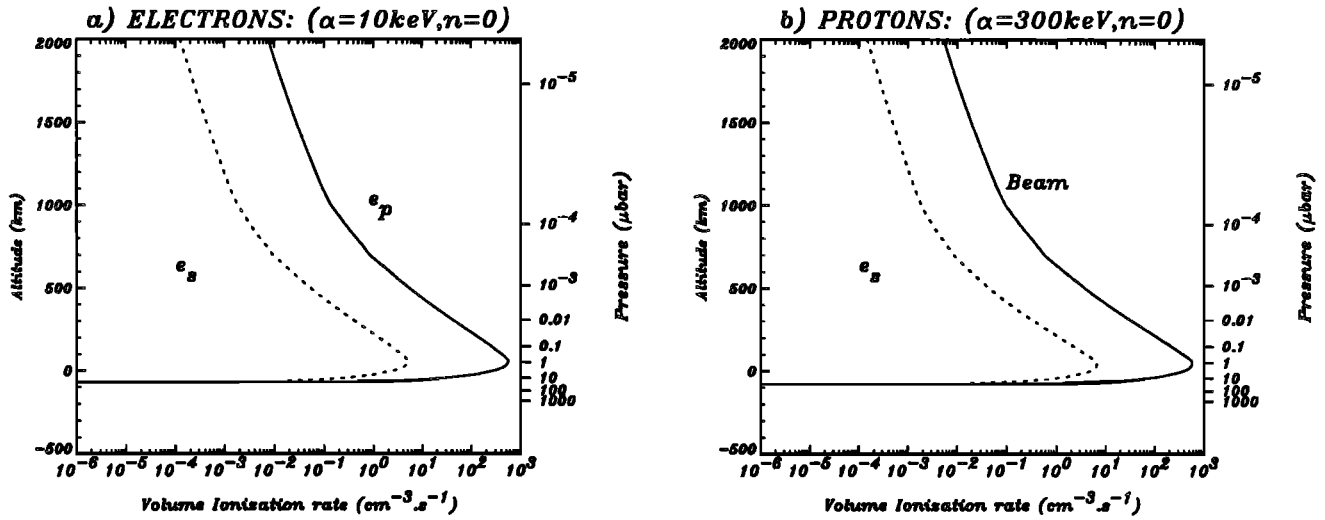

Figure 10. Comparison of the altitude distributions of the volume ionization rate due to the primary and secondary particles in the case of (a) a 10-keV electron incident beam and (b) a 300-keV proton incident beam.

Figure 11 compares the energy spectra of the secondary electrons created at three different levels in the atmosphere (near the top of the atmosphere at 2000 km, at 1000 km, and near the level of total degradation at 200 km) by an incident electron beam of initial energy 10 keV and by an incident proton beam of initial energy 300 keV. At all altitudes, the spectra exhibits a rather similar shape up to about 100 eV, with the absolute values of the differential flux larger in the case of proton primaries by a factor of about 1.3 than in the case of electron primaries. Above 100 eV, the secondary spectra decrease abruptly in the first case, whereas they exhibit a significantly high energy tail (up to more than 1 keV) when created by electron primaries.

By contrast, the volume excitation rates depend upon the nature of the precipitating particles. In Figure 12, we plot the contributions to the total excitation of H Lyman α (from atmospheric H and H_2) from the particles in the beam and from the secondary electrons. They differ by the relative secondary electron contribution. In the case of a proton aurora, the secondary electrons are the main contributor to the total excitation. And for an electron aurora, these secondary electrons represent about 58% of the total excitation rate (compared to 55% for the proton aurora).

Figure 13 shows the contributions of the primary and secondary particles to the volume excitation of the Lyman bands (results for the Werner bands are very close). They are more similar than in the case of H Lyman α. In both cases, the ratio of contributions from the beam and from the secondary electrons is roughly independent of altitude. These contributions are very close for the case of an incident electron beam (42.2% from the beam, 57.8% from the secondary electrons), whereas secondary electrons contribute slightly more for a proton beam (29.6% from the beam, 70.4% from the secondary electrons).

Finally, Figure 14 compares for incident electrons and protons the overall excitation rate of H Lyman α and of the H_2 bands, respectively. It appears that, although the volume excitation rate of H Lyman α and of the H_2 bands are quite similar at the top of the atmosphere in both cases, the ratio of volume excitation rates of H Lyman α to H_2 bands becomes smaller (by a factor 1.3) for the proton beam than for the electron beam in the region of the peak.

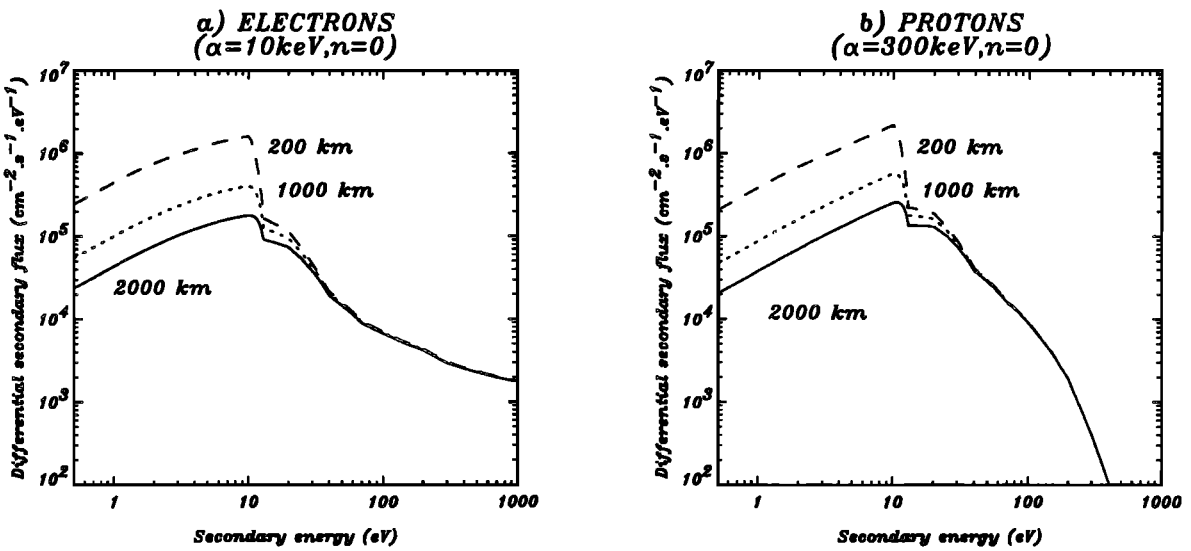

Figure 11. Energy spectra of the secondary electrons created at various altitudes in the atmosphere by (a) a 10-keV electron incident beam and (b) a 300-keV proton incident beam.

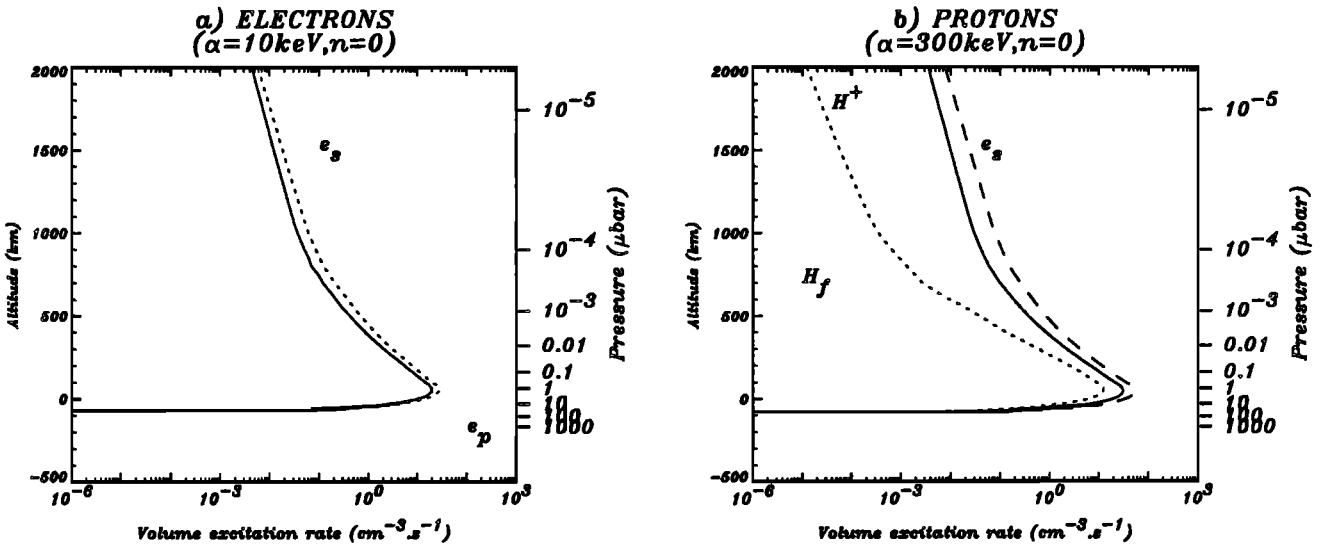

Figure 12. Same as Figure 10 for the excitation rate of H Lyman α.

5.3. Comparison of the Efficiency of a Proton and an Electron Aurora

In order to calculate the efficiencies (Table 2), we integrate the production rates over altitude for the principal processes in the case of a proton and an electron aurora. The contributions of the precipitating particles and of the secondary electrons are separated in both cases. The total energy input is 1 erg cm^{-2} s^{-1}. The fraction of the total energy deposited in the atmosphere via a given process (which represents the efficiency of this process) has also been calculated. Since we have only calculated the volume excitation rates, the column production rates represent the total number of quanta produced along the path by the precipitating particles. Cascading effects have been neglected for the estimation of the production of Lyman α coming from atmospheric H, but for the contribution coming from H_2, they have been taken into account in the experimental emission cross sections used. In the case of ionization, the column production rate is the number of ionizations produced by the particles during their degradation.

For the 300-keV proton aurora, the contribution of the secondary electrons to the Lyman and the Werner excitation is about 3 times the contribution of the protons of the beam, fast H contributing for less than 10% to the total. The fraction of the total energy input spent for the production of the H_2 bands is 24.5% versus 15.7% in the 10-keV electron aurora. For Lyman α (after addition of the contributions from H and H_2), the secondary electrons are responsible of about 56% of the total excitation. The fast H contribution is still of the order of 10%. For this range of initial energies, the excitation processes are essentially controlled by the secondary electrons. Ionization is the most important process, accounting for 27.1% of the total energy input. In this case, the secondary electrons do not play any significant role. Their contribution represents about 1% of the total. The ionization of the Jovian atmosphere is principally controlled by the precipitating beam.

We also compute the column production rates for the 10-keV electron aurora. For the Lyman and Werner band excitation, the contributions of the primary and secondary electrons are about

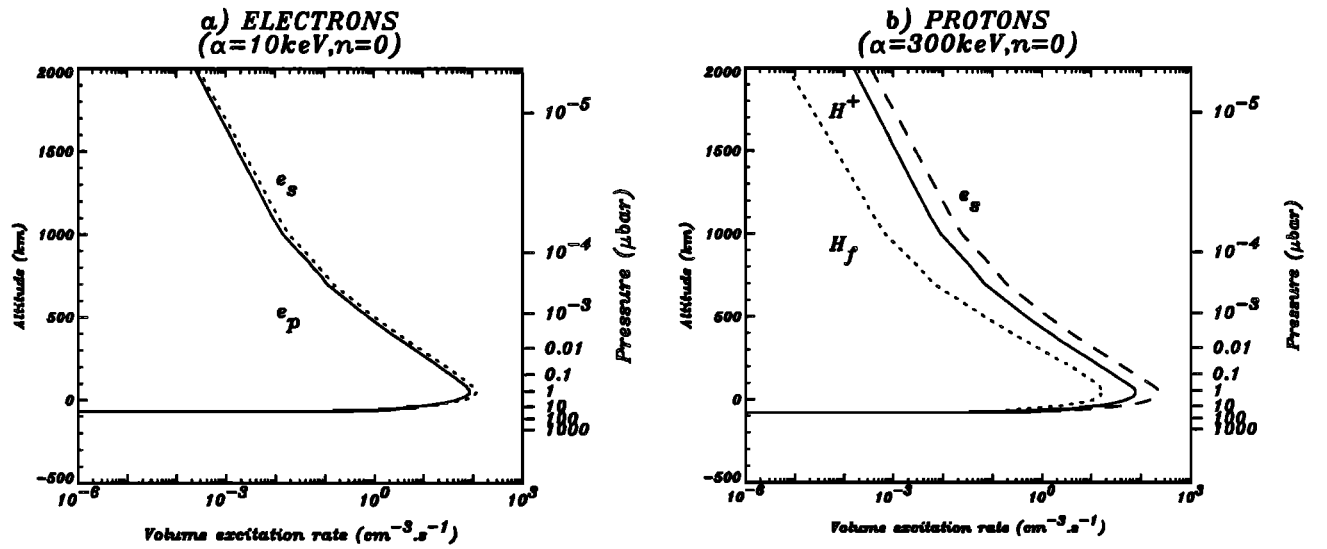

Figure 13. Same as Figure 10 for the excitation rate of the Lyman bands of H_2.

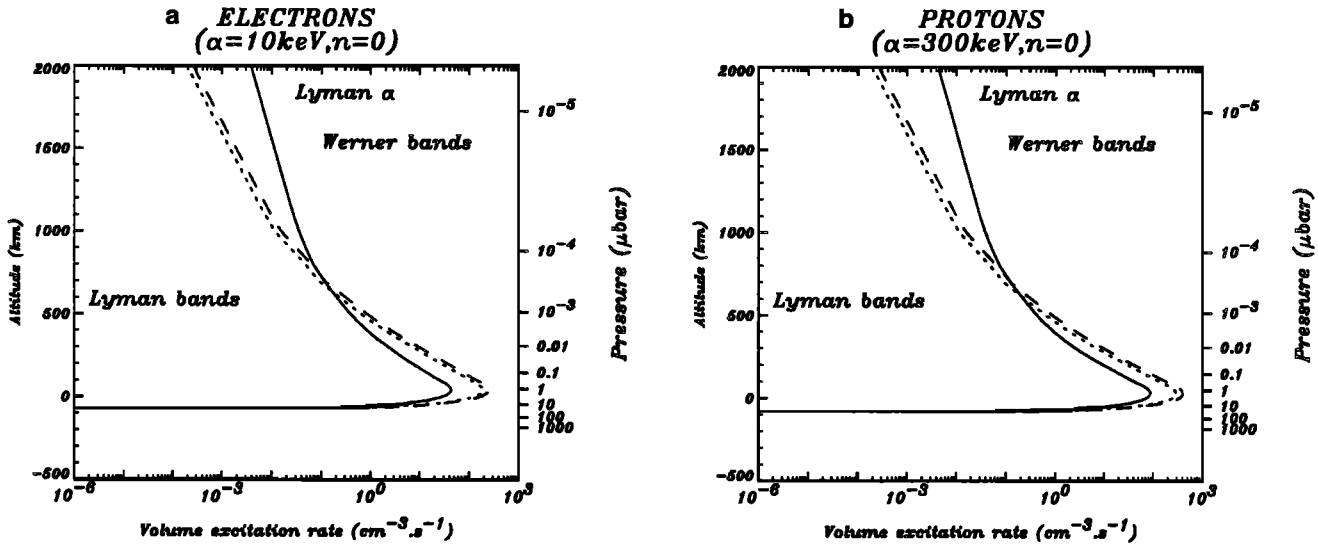

Figure 14. Comparison of the altitude distribution of the total excitation rate of H Lyman α and of the Lyman and Werner bands of H_2 by (a) a 10-keV electron incident beam and (b) a 300-keV proton incident beam.

60% and 40%, respectively. The contribution of the secondary electrons for the Lyman α excitation is about 1.3 times more than the primary contribution, as in the case of the 300-keV proton aurora where the secondary contribution is dominant. For ionization, the contribution of the secondary is negligible (less than 1% of the total), as for the proton aurora. But the 10-keV electron aurora is more efficient in ionizing the atmosphere (35.1% of the total energy input is spent for the ionization process) than the 300-keV proton aurora (only 27.1%). If we compare the overall fraction of the total energy spent in the ionization and excitation of the atmospheric constituents, we find that the 10-keV electrons are less efficient (52.8%) than the 300-keV proton aurora (55.3%).

A very rough estimate of the emergent intensities can be done. For a given line, the column production rate is proportional to the emergent intensity only if the atmosphere is strictly transparent for this line. Neglecting all the possible absorptions of the photons produced, which is, of course, not realistic, we find then that for 1 erg cm^{-2} s^{-1} and in the case of a 300-keV proton aurora, the emergent intensity in the H_2 bands (Lyman and Werner) would be 12.1 kR and 1.6 kR in the Lyman α line. In the case of the 10-keV electron aurora, the intensity in the H_2 bands would be 7.7 kR and 0.83 kR in the Lyman α line.

Gérard et al. [1993] deduced from recent observations of the Jovian FUV emissions with HST a value of 2.4 for the ratio R between the emergent intensity in the H_2 bands and at Lyman α (these data have not been obtained during the same observation and temporal variability of the auroral emissions can affect the value of R). Our model predicts a value of 7.6 for the 300-keV proton aurora and 9.3 for the 10-keV electron aurora. Our values are not realistic because the atmospheric extinction differs from line to line. However, they are not that far off the observed ratio. From the works of *Waite et al.* [1983], *Horanyi et al.* [1988] and *Shingal et al.* [1992], we can evaluate the ratio for different precipitating particles. We deduced from these papers the following values of R: 3.6 (10-keV electrons), 4.5 (ions S and O in the 100 keV range) and 7.8 (10-keV electrons), respectively. The particular high value of *Shingal et al.* [1992] is due to the low value of the excitation cross section of Lyman α by electron impact on H_2. This ratio R is, of course, energy dependent and its behavior is specific to the nature of the particles (Figure 15).

6. Effect of the Use of an Atmospheric Model

In order to investigate the effect of the atmospheric model adopted, we use the Jovian neutral atmosphere model of *Kim et al.* [1992] representative of an auroral zone. In such auroral models, the ionization of the atmospheric constituents (H and H_2) by precipitating particles produces molecular hydrogen ions which, through dissociation, create thermal neutral H. This is why in the Kim et al. model, the neutral H density is larger than in the McConnell model. In the Kim et al. model, we note also an increase of the molecular hydrogen density above the homopause in the altitude range of energy degradation due to the use of higher temperature. With an increase in the neutral densities, the volume excitation rates will also increase. In Figure 16, we plot the volume excitation rates of the H_2 bands (Lyman and Werner) and of Lyman α for precipitations of 10-keV electrons and 300-keV protons. The magnitude at the peak, which is less sharp, is of the same order as in the case of an equatorial model, and the precipitating particles produce more excitations and ionizations in the high-altitude region of the atmosphere because the densities have been increased. So the contribution of this region to the emergent intensity will increase, but only the application of a radiative transfer code would allow a precise determination of this contribution.

Using the model of Kim et al., we have calculated the ratio R defined in section 5.3. We have obtained a value for R of 5.6 for the 300-keV proton aurora and 5.9 for the 10-keV electron aurora. The influence of the neutral model is significant.

7. Conclusion

We have developed a code of energy degradation of protons applied to the Jovian aurorae. The method adopted is the continous slow down approximation. It is accurate enough for our study because we only consider beams of precipitating protons with high energies in comparison to the excitation and ionization threshold energies. This model allows the calculation of volume ionization and excitation rates of the H_2 bands (Lyman and Werner) and Lyman α. We have taken into account the charge exchange effects to evaluate these quantities.

Table 2. Comparison of the Efficiencies Between a 300-keV Proton and a 10-keV Electron Aurora

Process	300-keV Proton Aurora			Efficiency
	Column Production Rate			
	H_f	Protons	e_s^-	
H_2 ionization	9.3(9)		1.0(8)	27.1
H ionization	2.4(7)		9.2(5)	0.06
Lyman bands	2.7(8)	1.2(9)	3.6(9)	10.6 (5.1 kR)
Werner bands	3.8(8)	1.6(9)	4.9(9)	13.9 (7 kR)
Lyman α from H	6.8(5)	1.9(7)	5.6(7)	0.12 (76 R)
Lyman α from H_2	1.8(8)	4.8(8)	8.2(8)	3.5 (1.5 kR)

Process	10-keV Electron Aurora		Efficiency
	Column Production Rate		
	Primary electrons	e_s^-	
H_2 ionization	9.2(9)	8.3(7)	35.1
H ionization	3.1(7)	6.9(5)	0.11
Lyman bands	1.4(9)	1.9(9)	6.9 (3.3 kR)
Werner bands	1.8(9)	2.6(9)	8.8 (4.4 kR)
Lyman α from H	2.3(7)	4.4(7)	0.11 (67 R)
Lyman α from H_2	3.2(8)	4.4(8)	1.77 (7460 R)

Read 7.5(9) as 7.5 x 10^9 cm^{-2} s^{-1}. The emergent intensities are calculated without absorbtion by the hydrocarbons and without considering radiative transfer effects.

One of the results is that the beam of protons is not necessarily in an equilibrium state with respect to charge exchange, so that the use in such model of the formulas giving the equilibrium fraction of protons and fast H in the beam may not appropriate. This is due to the fact that the high-altitude region of the Jovian atmosphere is not sufficiently dense to ensure collisional equilibration of the precipitating beam. For an intermediate regime of initial energies of the precipitating protons (around 50 keV), the equilibration occurs close to the altitude of the peak volume excitation. It is in such a case that the charge exchange effects must be considered with care and in particular for the equilibration of the beam. We have distinguished different regimes of influence of the charge exchange. For high energies of the precipitating protons (greater than 200 keV), charge exchange does not affect the composition of the beam of incident protons, but for intermediate energies (10 keV to 200 keV), this process affects seriously the composition of the beam and we have to take into account the presence of fast H atoms (Figures 3 and 4). For the lowest energies (less than 10 keV), the charge exchange is dominant and the beam is dominantly neutral hydrogen. The results predicted by this code for energies lower than 10 keV have to be taken carefully because the validity of the assumptions of the CSDA method are no longer valid. Moreover, the cross section data we have used would have to be extrapolated below 10 keV.

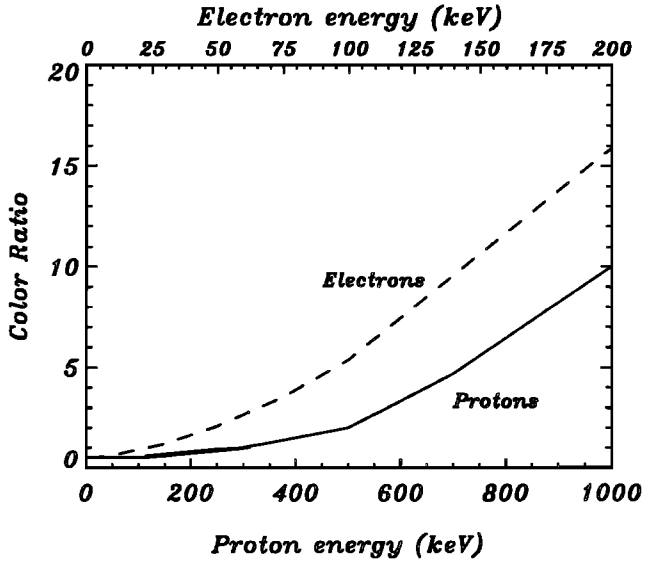

Figure 15. Ratio of the emergent intensity in the H_2 bands and at Lyman α for various energies (calculated without absorbtion and radiative transfer). Its behavior is specific to the nature of the precipitating particles.

We have also compared the volume ionization and excitation rates of the observed FUV emissions in the case of electron and proton precipitations. The secondary electrons, produced by ionization of the atmosphere, have a negligible contribution in the ionization process for the two types of aurorae. The ionization is controlled essentially by the precipitating particles. For the volume excitation rates, the secondary electrons, in the case of an electron aurora, contribute 58.4% to the total, whereas for a proton aurora, they become the main contributor (69% of the total) at all altitudes in the high-energy regime (>200 keV). For lower energies, fast H contribution to the excitation increases and becomes dominant at 50 keV. Comparing the volume excitation rates of the Lyman and the Werner bands to Lyman α for the two kinds of aurorae, we found that, for a given production of photons in the H_2 bands, the proton aurora produces more Lyman α than the electron aurora. But the effects of radiative transfer will affect this result. The ratio between the emergent intensity in the H_2 bands and at Lyman α is sensitive to the nature and energy of the precipitating particles. We expect to be able, with this model coupled with a radiative transfer code and by comparison with the observations, to predict this ratio. For the determination of the energy of the particles, it can be deduced from the value of the

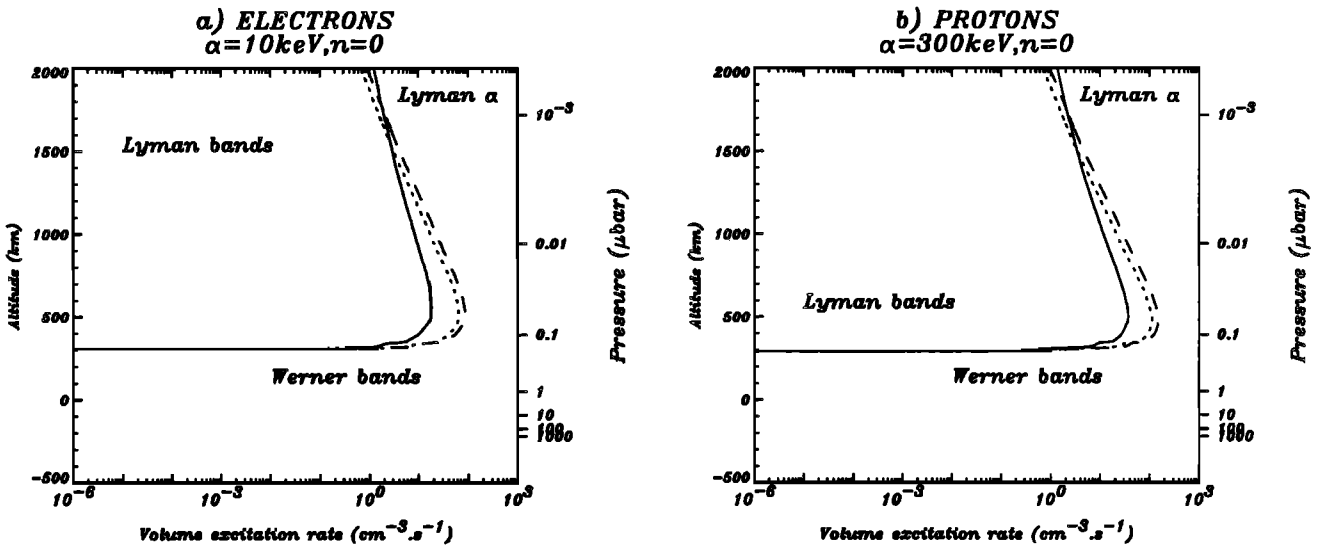

Figure 16. Same as Figure 14 with the auroral neutral model of *Kim et al.* [1992].

penetration depth determined by the ratio of the Lyman bands intensity and the Werner bands intensity (color ratio) as already done by *Gladstone and Skinner* [1989] and *Livengood and Moos* [1990]. Particle type can be deduced from the value of the ratio between the intensity in the H_2 bands and Lyman α intensity.

Appendix

In this section, we will deduce the local energy of the beam from equation (2). In the case of Jupiter, we have two atmospheric constituents. Equation (2) becomes

$$\left[\frac{dE}{dz}\right] = -\frac{n(z)}{\cos(\theta)}\left\{f_H(z)L_H(E) + f_{H_2}(z)L_{H_2}(E)\right\} \qquad \text{(A1)}$$

where $n(z)$ is the altitude profile of the total density, $L_s(E)$ is the loss function of protons in the gas s and $f_s(z)$ is the fractional abundance of the gas s. According to the results of *Phelps* [1990], we assume identical loss function for protons and H in H_2. And in the separated atom model, we have

$$L_{H_2}(E) = 2L_H(E) \qquad \text{(A2)}$$

Since the sum of the fractional abundances of the species composing the atmosphere is equal to unity, (A1) becomes

$$\left[\frac{dE}{dz}\right] = -\frac{n(z)L_{H_2}(E)}{2\cos(\theta)}\left\{1 + f_{H_2}(z)\right\} \qquad \text{(A3)}$$

We have adopted for $L_H(E)$ the analytical form of *Green and Peterson* [1968]. Then we can easily integrate (A3), i.e.;

$$\int_{E_0}^{E(z=h)=E_{loc}(h,\theta)} \frac{dE}{L_{H_2}(E)} = -\frac{1}{2\cos(\theta)} \int_{\infty}^{z=h} \left\{1 + f_{H_2}(z)\right\} n(z)dz \qquad \text{(A4)}$$

Inverting this equation numerically will give us the local energy of the beam, which is altitude and pitch angle dependent.

Acknowledgments. The authors want to acknowledge fruitful discussions with J. Lilensten on the CSDA versus multistream codes, and with Jack McConnell on the atmospheric photochemical and excitation processes. We want also to thank Jack McConnell for providing the atmospheric model used in this study. Many thanks also to A.V. Phelps for helpful discussions about the loss functions. One of the authors (J.C.G.) acknowledges support from the Belgian National Fund for Scientific Research (FNRS). Partial support for this research comes from CNRS/INSU grant ATP Planétologie 89-37-08.

References

Ajello, J. M., D. E. Shemansky, and G. K. James, Cross sections for production of H(2*p*, 2*s*, 1*s*) by electron collisional dissociation of H_2, *Astrophys. J.*, *371*, 422-431, 1991.

Allison, S.K., Experimental results on charge-changing collisions of hydrogen and helium atoms and ions at kinetic energies above 0.2 keV, *Rev. Mod. Phys.*, *30*, 1137-1168, 1958.

Armstrong, T.P., M.T. Paonessa, S.T. Brandon, S.M. Krimigis, and L.J. Lanzerotti, Low energy charged particle observations in the 5-20 RJ region of the Jovian magnetosphere, *J. Geophys. Res.*, *86*, 8343-8355, 1981.

Balogh, M.K., M.K. Dougherty, R.J. Forsyth, D.J. Southwood, E.J. Smith, B.T. Tsurutani, N. Murphy, and M.E. Burton, Magnetic field observations during the Ulysses flyby of Jupiter, *Science*, *257*, 1515-1518, 1992.

Barbosa, D. D., Bremsstrahlung X rays from Jovian auroral electrons, *J. Geophys. Res.*, *95*, 14,969-14,976, 1990.

Barbosa, D.D., F.L. Scarf, W.S. Kurth, and D.A. Gurnett, Broadband electrostatic noise and field-aligned currents in Jupiter's middle magnetosphere, *J. Geophys. Res.*, *86*, 8357-8369, 1981.

Belcher, J. W., C. K. Goertz, J. D. Sullivan, M. H. Acuna, and N. F. Ness, Plasma observations of the Alfven wave generated by Io, *J. Geophys. Res.*, *86*, 8508-8512, 1981.

Birely, J.H., and R. J. McNeal, Formation of H(2p) and H(2s) in collisions of protons and hydrogen atoms with hydrogen molecules, *Phys. Rev. A Gen. Phys.*, *5*, 692-701, 1972.

Blake, J. B., E. Keppler, A. Korth, M. Witte, J. J. Quenby, D. Hovestadt, and J. Woch, Composition aspects during the Jupiter flyby of Ulysses, paper presented at the XVII General Assembly of EGS, Edinbourg (UK), April 6-10, 1992.

Broadfoot, A.L., et al., Extreme ultraviolet observations from Voyager 1 encounter with Jupiter, *Science*, *204*, 979-982, 1979.

Cheng, A. F., M. T. Paonessa, and T. P. Armstrong, Energetic ion losses near Io's orbit, *J. Geophys. Res.*, *88*, 3936-3944, 1983.

Clarke, J.T., H.W. Moos, S.K. Atreya, and A.L. Lane, Observations from Earth orbit and variability of the polar aurora on Jupiter, *Astrophys. J., 241*, L179-182, 1980.

Cravens, T.E., G. A. Victor, and A. Dalgarno, The absorption of energetic electrons by molecular hydrogen gas, *Planet. Space Sci., 23*, 1059-1070, 1975.

Dols, V., J.C. Gérard, F. Paresce, R. Prangé, and A. Vidal-Madjar, Ultraviolet imaging the Jovian aurora with the Hubble Space Telescope, *Geophys. Res. Lett., 19*, 1803-1806, 1992.

Edgar, B.C., W. T. Miles, and A. E. S. Green, Energy deposition of protons in molecular nitrogen and applications to proton auroral phenomena, *J. Geophys. Res., 78*, 6595-6606, 1973.

Edgar, B.C., H. S. Porter, and A. E. S. Green, Proton energy deposition in molecular and atomic oxygen and applications to the polar cap, *Planet. Space Sci., 23*, 787-804, 1975.

Festou, M., S. K. Atreya, T.M. Donahue, B.R. Sandel, D.E. Shemansky, and A.L. Broadfoot, Composition and temperature profiles of the Jovian upper atmosphere detrmined by the Voyager ultraviolet stellar occultation experiment, *J. Geophys. Res., 86*, 5715-5725, 1981.

Garvey, R.H., H. S. Porter, and A. E. S. Green, Relativistic yield spectra for H_2, *J. Appl. Phys., 48*, 4353-4359, 1977.

Gealy, M.W., and B. Van Zyl, Cross sections for electron capture and loss, I, H^+ and H^- impact on H and H_2, *Phys. Rev. A Gen Phys., 36*, 3091-3099, 1987a.

Gealy, M.W. and B. Van Zyl, Cross sections for electron capture and loss, II, H impact on H and H_2, *Phys. Rev. A Gen. Phys., 36*, 3100-3107, 1987b.

Gehrels, N., and E.C. Stone, Energetic oxygen and sulfur ions in the Jovian magnetosphere and their contribution to the auroral excitation, *J. Geophys. Res., 88*, 5537-5550, 1983.

Geiss, J., G. Gloeckler, H. Balsiger, L.A. Fisk, A.B. Galvin, F. Gliem, D.C. Hamilton, F.M. Ipavich, S. Livi, U. Mall, K.W. Ogilvie, R. von Steiger, and B. Wilken, Plasma composition in Jupiter's magnetosphere: Initial results from the solar wind ion composition spectrometer, *Science, 257*, 1535-1538, 1992.

Gérard, J.C., and V. Singh, A model of energy deposition of energetic electrons and EUV emission in the Jovian and Saturnian atmospheres and implications, *J. Geophys. Res., 87*, 4525-4532, 1982.

Gérard, J.C., V. Dols, F. Paresce, and R. Prangé, Morphology and time variation of the jovian far UV aurora: Hubble Space Telescope observations, *J. Geophys. Res., 98*(E10), 18,793-18,801, 1993.

Gladstone, G.R., and T. E. Skinner, Spectral analysis of Jovian auroral emissions, Time-Variable Phenomena in the Jovian System, *NASA Spac. Publ., SP-494*, pp.221, 1989.

Goertz, C. K., Proton aurora on Jupiter's nightside, *Geophys. Res. Lett., 7*, 365-368, 1980.

Green, A.E.S., and R. J. McNeal, Analytic cross sections for inelastic collisions of protons and hydrogen atoms with atomic and molecular gases, *J. Geophys. Res., 76*, 133-144, 1971.

Green, A.E.S., and L. R. Peterson, Energy loss for electrons and protons in planetary gases, *J. Geophys. Res., 73*, 233-241, 1968.

Green, A.E.S., and T. Sawada, Ionization cross sections and secondary electron distributions, *J. Atmos. Terr. Phys., 34*, 1719-1728, 1972.

Halthore, R., A. Burrows, and J. Caldwell, Infrared polar brightenings on Jupiter, *Icarus, 74*, 340-350, 1988.

Heaps, M.G., B. C. Edgar, and A. E. S. Green, Jovian proton aurora, *Icarus, 24*, 78-85, 1975.

Horanyi, M., T.E. Cravens, and J.H. Waite, Jr., The precipitation of energetic heavy ions into the upper atmosphere of Jupiter, *J. Geophys. Res., 93*, 7251-7271, 1988.

Hughes, R.H., T. J. King, and S-S Choe, Cross sections for the production of Lyman-α radiation by fast-proton impact on H_2, *Phys. Rev. A Gen. Phys., 5*, 644-647, 1972.

Janev, R. K., W. D. Langer, K. Evans, Jr., and D. E. Post, Jr., Elementary processes in hydrogen-helium plasmas: cross sections and reaction rate coefficients, Springer-Verlag, New York,1987.

Kim, Y. H., J.L. Fox, and H.S. Porter, Densities and vibrational distribution of H_3^+ in the Jovian auroral ionosphere, *J. Geophys. Res., 97*, 6093-6101, 1992.

Kostiuk, T., F. Espenak, M.J. Mumma, D. Deming, and D. Zipoy, Variability of ethane on Jupiter, *Icarus, 72*, 394-410, 1987.

Krimigis, S. M., et al., *Science, 204*, 998-1003, 1979.

Lanzerotti L.J., C.G. McLennan, T.P. Armstrong, S.M. Krimigis, R.P. Lepping, and N.F. Ness, Ion and electron angular distributions in the Io torus region of the Jovian magnetosphere, *J. Geophys. Res., 86*, 8491-8496, 1981.

Lanzerotti, L.J., et al., The hot plasma environment of Jupiter: Ulysses results, *Science, 257*, 1518-1524, 1992.

Le Quéau, D., R. Pellat, and A. Roux, Direct generation of the auroral kilometric radiation by the maser synchrotron instability: An analytical approach, *Phys. Fluids, 247*, 1984.

Lin, N. P., J. Kellog, R. J. MacDowall, Y. Mei, N. Cornilleau-Wehrlin, P. Canu, C. De Villedary, L. Rezeau, A. Balogh, and R. J. Forsyth, ULF waves in the Io torus: Ulysses observations, *J. Geophys. Res.*, in press, 1993.

Livengood, T.A., and H.W. Moos, Jupiter's north and south polar aurorae with IUE data, *Geophys. Res. Lett., 17*, 2265-2268, 1990.

Livengood, T.A., H.W. Moos, G.E. Ballester, and R. Prangé, Jovian ultraviolet auroral activity, 1981-1991, *Icarus, 97*, 26-45, 1992.

Louarn, P., A. Roux, H. de Feraudy, D. Le Quéau, M. André, and L. Matson, Trapped electrons as a free energy source for the AKR, *J. Geophys. Res., 95*, 5983-5996, 1990.

Mayo, R., S. Rolston, and T. J. Morgan, Born and impact-parameter cross sections for the process : H(1s)+H(1s) → H(2s)+H(1s), *Can. J. Phys., 66*, 645-648, 1988.

McClure, G.W., Ionization and electron transfer in collisions of two H atoms : 1.25-117 keV, *Phys. Rev., 166*, 22-29, 1968.

Metzger, A.E., D.A. Gilman, J.L. Luthey, K.C. Hurley, H.W. Schnopper, F.D. Seward, and J.D. Sullivan, The detection of X-rays from Jupiter, *J. Geophys. Res., 88*, 7731-7741, 1983.

Miller, J.H., and A. E. S. Green, Proton energy degradation in water vapor, *Radiation Res., 54*, 343-363, 1973.

Morgan, T.J., J. Stone, and R. Mayo, H(2s) formation in H^+-H and H-H collisions, *Phys. Rev. A Gen. Phys., 22*, 1460-1466, 1980.

Olivero, J.J., J. N. Bass, and A. E. S. Green, Photoelectron excitation of the Jupiter dayglow, *J. Geophys. Res., 78*, 2812-2826, 1973.

Opal, C.B., W. K. Peterson, and E. C. Beaty, Measurements of secondary-electron spectra produced by electron impact ionization of a number of simple gases, *J. Chem. Phys., 55*, 4100-4106, 1971.

Paonessa, M., Voyager observations of ion phase space densities in the Jovian magnetosphere, *J. Geophys. Res., 90*, 521-525, 1985.

Phelps, A.V., Cross sections ans swarm coefficients for H^+,H_2^+,H_3^+,H,H_2 and H^- in H_2 for energies from 0.1 to 10 keV, *J. Phys. Chem. Ref. Data, 19*, 653-675, 1990.

Prangé, R., The Jovian UV aurorae, IR aurorae, and particle precipitations: A common origin?, *Astron. Astrophys., 251*, L15, 1991.

Prangé, R., and M. Elkhamsi, Modeling the precipitation flux in the Jovian auroral zones, 1 The model and its application to the UV auroral emissions, *J. Geophys. Res., 96*, 21,371-21,389, 1991.

Prangé, R., D. Rego, and J.C. Gérard, Auroral Lyman α and H_2 bands from the giant planets: 2. Effect of the anisotropy of the precipitating particles on the interpretation of the 'color ratio', Submitted to JGR-Planets, 1994.

Rees, M.H., A. I. Stewart, and J. C. G. Walker, Secondary electrons in aurora, *Planet. Space Sci., 17*, 1997-2008, 1969.

Rudd, M.E., Energy and angular distributions of secondary electrons from 5-100 keV proton collisions with hydrogen and nitrogen molecules, *Phys. Rev. A Gen. Phys., 20*, 787-796, 1979.

Sandel, B. R., et al., Extreme ultraviolet observations from Voyager 2 encounter with Jupiter, *science, 206*, 962-966, 1979.

Shingal, R., B. H. Bransden, and D. R. Flower, Formation of H(2s) and H(2p) in collisions between ground-state hydrogen atoms, *J. Phys. Condens. Matter, 20*, L477-L480, 1987.

Shingal, R. P., S. C. Chakravarty, A. Bhardwaj, and B. Prasad, Energetic electron precipitation in Jupiter's upper atmosphere, *J. Geophys. Res., 97*, 18,245-18,256, 1992.

Simpson, J.A., et al., Energetic charged particles phenomena in the Jovian magnetosphere: First results from the Ulysses COSPIN collaboration, *Science, 257*, 1543-1550, 1992.

Summers D., R.M. Thorne, and Y. Mei, Jupiter's radiation belt ions: A comparison of theory and observation, *Geophys. Res. Lett., 16*, 231-234, 1989.

Swartz, W.E., J. S. Nisbet, and A. E. S. Green, Analytic expression for the energy-transfer rate from photoelectrons to thermal-electrons, *J. Geophys. Res., 76*, 8425-8426, 1971.

Thomsen, M.F., C.F. Goertz, and J.A. Van Allen, On determining magnetospheric diffusion coefficients from the observed effects of Jupiter's satellite Io, *J. Geophys. Res. 82*, 5541-5549, 1977.

Thorne, R. M., Jovian auroral secondary electrons and their influence on the Io plasma torus, *Geophys. Res. Lett., 8*, 509-512, 1981.

Thorne, R.M., Microscopic plasma processes in the Jovian magnetosphere, in *Physics of the Jovian Magnetosphere*, edited by Dessler, pp. 454-488, Cambridge University Press, New York, 1983.

Thorne, R.M., and F.L. Scarf, Voyager 1 evidence for ion-cyclotron instability in the vicinity of the Io plasma torus, *Geophys. Res. Lett., 11*, 263-266, 1984.

Trafton, L., Several early results from HST planetary observations, Symposium on HST, Chia Laguna (Italy), June 29-July 7, 1992.

Van Zyl, B., M. W. Gealy and H. Neumann, Lyman-α emission from low-energy $H+H_2$ and $H^+ + H_2$ collisions, *Phys. Rev. A Gen. Phys., 40*, 1664-1666, 1989.

Waite, J.H., Jr., and D.C. Boice, Multi-spectrral observations of the Jovian aurorae, Paper presented at Workshop on 'Variable Phenomena in Jovian Planetary Systems', Am. Astron. Soc., Annapolis, M., July 13-16, 1992.

Waite, J.H., Jr., T.E. Cravens, J. Kozyra, A.F. Nagy, S.K. Atreya, and R.H. Chen, Electron precipitation and related aeronomy of the Jovian thermosphere and ionosphere, *J. Geophys. Res., 88*, 6143-6163, 1983.

Waite, J.H., Jr., J.T. Clarke, T.E. Cravens, and M.C. Hammond, The Jovian aurora : Electron or ion precipitation? *J. Geophys. Res., 93*, 7244-7250, 1988.

Wu, C.S., H.K. Wong, D.J. Gorney, and L.C. Lee, Generation of the auroral kilometric radiation, *J. Geophys. Res., 87*, 4476-4488, 1982.

Yung, Y. K., G. R. Gladstone, K. M. Chang, J. M. Ajello, and S. K. Srivastava, H_2 fluorescence spectrum from 1200 to 1700 Å by electron impact: laboratory study and application to Jovian aurora, *Astrophys. J., 254*, L65-L69, 1982.

J.C. Gérard, Institut d'Astrophysique de Liège, 5 Avenue de Cointe, 4000 Liège, Belgium. (e-mail: gerard@geo.astro.ulg.ac.be)

R. Prangé and D. Rego, Institut d'Astrophysique Spatiale, Bâtiment 121, Université Paris XI, 91405 Orsay, France. (e-mail: prange@ias.fr; rego@ias.fr)

(Received February 24, 1993; revised November 16, 1993;
accepted December 3, 1993.)